Effects of the Laplace pressure and of gas pressure on isostatic pressing and free sintering of cylindrical specimens.

L. Galuppi[1], L. Deseri[2]

[1] *Industrial Engineering Dept., University of Parma, Parma, Italy*
[2] *D.I.M.S., Mechanical and Structural Engineering Dept., University of Trento, Trento, Italy*
E-mail: laura.galuppi@unipr.it
E-mail: luca.deseri@ing.unitn.it

Abstract

DA RISCRIVERE Unlike previous recent contributions [20], the influence of the gas pressure in pores and of local capillary stresses acting at the surface of one pore or particle (called *interstitial stress* or *Laplace pressure*) during sintering of pre-compacted metallic (micro/nano)-powdered cylinders is here analyzed. In this paper, the isostatic pressing loading mode, which also covers the case of free sintering, is considered.

The role of the Laplace pressure is twofold.

- First of all, during the sintering process such a pressure influences the evolution of the porosity and, for instance, its residual value at a given time. It is worth emphasizing that threshold pressures are determined below which the sintering stress is actually not negligible; the duration of the process is indeed heavily affected by such a stress whenever the residual porosity is prescribed. In turn, such a duration would be underestimated otherwise. Furthermore, industrial processes often entail loading pressures lower than the thresholds mentioned above, especially of "small" grain sizes.
- In the case of isostatic pressing with non-null external load, the loading parameter may be tuned in such a way that, at some stage of the process, i.e. when a "critical porosity" is reached, its value may equate the Laplace pressure. Henceforth, the porosity would remain constant.

  A stability analysis allows us to conclude that, the equilibrium is unstable at such a value and hence the sintering may keep on going.

  It follows that in order to have stability of sintering either the loading parameter must be high enough with respect to the Laplace pressure or it must be zero, which would give rise to (stable) free sintering.

Notation

σ_{ij} = components of the stress tensor
$\dot{\varepsilon}_{ij}$ = components of the strain rate tensor
$\dot{\varepsilon}'_{ij}$ = components of the deviatoric strain rate tensor
$\dot{e}$= first invariant of the strain rate tensor
p_L= Laplace pressure (sintering stress)
p_i=gas pressure in pores
w= effective equivalent strain rate
θ= porosity
ψ= normalized bulk modulus
φ= normalized shear modulus
$\dot{\gamma}$= second invariant of the deviatoric strain rate tensor
p= first invariant of the stress tensor
τ= second invariant of the stress tensor
σ_r= radial stress
σ_z= axial stress
$\dot{\varepsilon_r}$= radial strain rate
$\dot{\varepsilon_z}$= axial strain rate
n^*= loading mode parameter
n= strain rate mode parameter
$\sigma(w)$= effective equivalent stress
σ_0= reference stress
$\dot{\varepsilon_0}$= reference strain rate
A= time-dependent material constant
m= strain rate sensitivity
ρ= relative density
V_{tot}= total volume of sintered material
V_{matrix}= matrix volume
V_{pores}= pores volume
τ_L= dimensionless specific time
$S.E.P.$= specific external pressure
α= surface tension
r_0= characteristic radius of particles
p_{l0}= reference value of the Laplace pressure
R_1, R_2= internal and external radius of the hollowed sphere considered as a schematic for a pore, respectively
V_r= radial velocity
D= dissipation potential
θ_c= closure porosity
p_{atm}= atmospheric pressure
t= sintering time evaluated by accounting for the Laplace pressure
t_0= sintering time evaluated by neglecting the Laplace pressure
$p*$= external pressure for which a given value of the discrepancy between t and t_0 is obtained
θ_r= residual porosity at the end of the sintering process, evaluated by accounting for the Laplace pressure
θ_{r0}= residual porosity at the end of the sintering process, evaluated by neglecting the Laplace pressure
e= error on the evaluation on the residual porosity
θ_F= desired final porosity at the end of the sintering process
θ^*= limit value of the porosity

λ= perturbation growth rate
$\bullet^{(0)}$= reference solution for ($\bullet$)
$\delta\bullet$= perturbation of ($\bullet$)

1. Introduction

In the last decades, powder technology has become one of the most important technological processes for the production of metallic and ceramics components; free sintering, hot isostatic pressing and hot forging are different ways to realize a key-phase in which the primary mechanical properties of the final material are obtained. In order to be able to predict the final structure of a body undergoing such a kind of process, it is crucial to define an analytical theory of sintering allowing to follow the evolution of the mechanical properties of the material (determined by this structure) during sintering and to get the final features of the compound at the end of this process.
Since the foundations of the analytical study of sintering processes have been laid in the seventies (see, for example, [26, 1, 6]) and many studies have given important new impulses in the nineties [19, 4, 7], even in last years several paper have been improve the knowledge of sintering processes, both from the analytical (see, among others, [21, 32, 15]) and the experimental (see, for example, [10, 23]) point of view; the latter is usually many focused on new materials and techniques. An innovative sintering technique, widely developed and used in last years, is the Spark Plasma Sintering (SPS), in which materials are compacted and condensed into higher densities. Systems designed for spark plasma sintering use direct current pulses to create spark energy between the particles of the material. This technology achieves fast fusing between particles and, unlike other sintering processes that are solely involved in metalworking, spark plasma sintering can be applied to ceramics, composite materials, and nanostructures. The compaction of the material can be achieved in a relatively short time period, making the SPS a very promising technique to elaborate nanostructured materials and several studies have been performed, in last years, about this technique [17, 28, 34].

The present work is focused on modeling the evolution of material properties during sintering of axisymmetric samples, and it is a natural extension of [20], dealing with an analysis of the kinetics and the stability of porous axially symmetric bodies undergoing sintering under different loading modes. In such a paper, besides an extensive review of the available literature, both about modeling of sintered material obtained by compacted powders and constitutive equations for porous media, the problem is solved for the cases in which both the interstitial stress (due to the pressure exerted by the gas in the pores) and the Laplace pressure (due to the surface tension at the interfaces between matrix and pores) are negligible compared with the one due to external loading. On the other hand, the strategy introduced in [20] appears to be the most effective one among other possibilities in order to predict the kinetics of bodies undergoing sintering (even for simple geometry mentioned above).

Even if sintering is an inhomogeneous process, thanks not only to inhomogeneity of properties of the powder particles but also to internal stresses can arise from external constraint or from differential densification [9] or particle rearrangement during sintering [31, 13], in this work only the average state of stress is considered. This is motivated by the observation, pointed out by Olevsky and Molinari [20], that the assumption of homogeneous plane stress through a sample is reasonable even in the

case of non-uniform cross-section (see e.g. [11] for tensile tests). Incidentally, this is equivalent to assuming that specimens undergo constant states of (plane) stresses corresponding to the average of the actual stress fields. The approach suggested by the assumptions above has the advantage of capturing the essentials of both kinetics and stability, avoiding to search for the solution of complicated (initial) boundary value problems. Nevertheless, in [20], this strategy has been employed only for the cases in which the effect of the Laplace pressure is negligible with respect to the applied stresses. Hence it needs to be extended to the case of moderate stresses in comparison with the interstitial gas pressure.
evidenziare che qui consideriamo un processo a stress costante (e non a carico fittizio esterno costante), che pi realistico
This paper may be outlined as follows.
In Section 2, the theory of sintering introduced in [18, 20] is essentially summarized and specialized for the case of isostating pressing processes, emphasizing the role of the Laplace pressure and the gas pressure in pores. In Sect. 2.3, the two most used ways to get the relationship between the porosity and the Laplace pressure (also denoted as *sintering stress*)are revisited; furthermore, the model for obtaining such a pressure based on the microscopic dissipation is shown to be compatible with the incompressibility of the matrix if and only if the material is nonlinearly viscous. Analogously, in Sect. 2.4 a practical way to account for the interstitial stress (i.e.the gas pressure in pores) is proposed.
In Section 3, the effect of the Laplace pressure on the evolution of the porosity in sintering processes entailing isostatic-pressing is studied. An accurate comparison among different models for the shear and bulk moduli of the material and between the two different expressions for the sintering is performed. Furthermore, in 3.1, two issues are investigated. First of all, thresholds on stresses cased by external loads are determined under which the influence of the interstitial pressure cannot be neglected. Such thresholds may strongly be influenced by the strain rate sensitivity of the material and the averaged radius of the particles; this feature may have a stronger impact for nanostructured powders. Furthermore, the discrepancy between the values of the residual porosity is evaluated by neglecting or accounting for the Laplace pressure in sintering processes of a given time-duration. In Sect. 4, an analog analysis is perform regarding the effect of gas pressure in pores in isostating pressing sintering processes. In performing such analysis, two cases may arise through a comparison between the stress caused by external loading and Laplace pressure (driving sintering) and gas pressure in pores (opposing to the reduction of the porosity). In particular, the occurrence of equality between such values can be reached at a definite (critical) porosity, which remains constant at a limit value. It is clear that, if such value is major than the desired porosity at the end of the process, this cannot be obtained.
Finally, in Section 5, the stability of the process, namely of the solution of the problem in terms of time evolution of the porosity obtained in Sect. 2, is performed in two steps along the lines traced in [20]. A lower order analysis is performed in Sect. 5.1, where perturbations on the porosity alone are considered. In Sect. 5.2 and 5.3, a higher order analysis is performed by perturbing, together with the porosity, the reference value of the Laplace pressure and the gas pressure in pores; this more refined analysis shows that effect of the latter is to reduce the stability of the process. Appendix A is devoted to analyze free sintering processes. In particular, since no external stress is applied, it is crucial to examine to what extend different ways to evaluate the laplace pressure may influence the outcome in terms of evolution of the porosity. Henceforth, a parametric analysis in terms of the given temperature is performed to estimate the

sintering time for a prescribed target residual porosity.

2. Theory of sintering and kinetics of the porosity

The sintering process is classically divided into three phases ([4, 29, 30]):

- a first stage in which the particles are brought into contact and necks grow at the particle contacts; in this phase, the material may be modeled as an aggregate of individual particles with small contact; for crystalline materials, this phase involves diffusion of vacancies in the crystal lattice, whereas noncrystalline materials sinter by viscous flow [25];
- an intermediate stage (second stage) in which the material can be idealized as a porous material with connected porosity;
- a third (final) phase in which, usually for relative densities greater than 90% [6], i.e. for porosity less than 10%, in which the pores are isolated and spherical. In the sequel, such a value of porosity will be denoted by $\theta_c = closure\ porosity$.

It is important to note that in the second phase the pores can be considered quasi-spherical (see [1]).

theory

The mechanical response of a porous body with nonlinear-viscous behavior (stage 2 and 3) are strongly influenced by the presence of pores (see, for example, the recent contribution by Wakai [32]) and it is described by a rheological constitutive relation, namely:

$$\sigma_{ij} = \frac{\sigma(w)}{w}[\varphi\dot{\varepsilon}'_{ij} + \psi\dot{e}\delta_{ij}] + p_L\delta_{ij} - p_i\delta_{ij}, \tag{1}$$

legame

inter-relating the components of the stress σ_{ij} and the strain rate $\dot{\varepsilon}_{ij}$[18].

The quantity p_L represents the Laplace pressure, whereas the term p_i represent the gas pressure in the pores. Obviously, $p_i = 0$ during first and second phases, since the porosity is open.

Here, $\dot{\varepsilon}'_{ij}$ denotes the i-j-th component of the deviatoric strain rate tensor; w is the effective equivalent strain rate, defined as follows:

$$w = \frac{1}{\sqrt{1-\theta}}\sqrt{\varphi\dot{\gamma}^2 + \psi\dot{e}^2}, \tag{2}$$

w

where

$$\dot{e} = \dot{\varepsilon}_{ii} \tag{3}$$

e

measures the local shrinking rate (whenever the sintering process entails a volume reduction), and

$$\dot{\gamma} = \sqrt{\dot{\varepsilon}'_{ij}\dot{\varepsilon}'_{ij}} \tag{4}$$

gamma

measures the local rate of change in shape (i.e. it is the second invariant of the deviatoric strain rate tensor).

The quantity p_L represents the interstitial pressure produced by the gas contained in the pores; in the sequel we shall refer to p_L as either the "Laplace pressure" or the "sintering stress" (see [20, 19, 18]).

For further developments, it is convenient to introduce the stress quantities p, τ directly related to shrinking and change in shape, respectively, i.e.:

$$p = \frac{1}{3} tr\sigma = \frac{\sigma(w)}{w}\psi\dot{e} + p_L - p_i, \tag{5}$$ p

$$\tau = \sqrt{\sigma'_{ij}\sigma'_{ij}} = \frac{\sigma(w)}{w}\varphi\dot{\gamma}. \tag{6}$$ tau

The quantities φ, ψ, p_L and their dependence upon the porosity will be treated in sections 2.1 and 2.2.
Let us consider a cylindrical axisymmetric specimen, subject to an external load. The porosity θ, defined as the ratio between the pores volume and the total volume (see [20]), is supposed to be constant throughout the sample. This is equivalent to consider the space-average of the porosity.

From now on, we shall consider averaged stress distributions of the following form:

$$[\sigma_{ij}] = \begin{bmatrix} \sigma_r & 0 & 0 \\ 0 & \sigma_r & 0 \\ 0 & 0 & \sigma_z \end{bmatrix}, \tag{7}$$ stresstensor

where z denotes the direction of the axis of the sample and r is any radial direction. Furthermore, in the sequel, the corresponding averaged strain rate tensor will be considered.
Here, $\dot{\varepsilon}_z$ and $\dot{\varepsilon}_r$ denote the axial and radial strain rates, respectively. Henceforth, the first and second invariants of the strain rate tensor turn out to be:

$$\dot{e} = \dot{\varepsilon}_z + 2\dot{\varepsilon}_r, \qquad \dot{\gamma} = \sqrt{\frac{2}{3}}|\dot{\varepsilon}_z - \dot{\varepsilon}_r|. \tag{8}$$ egamma

Following Olevsky and Molinari [20], one can introduce a loading mode parameter n^* defined by:

$$n^* = \frac{\tau}{p} = \frac{\varphi\dot{\gamma}}{\psi\dot{e} + p_L - p_i}. \tag{9}$$ n*

In analogy to the loading mode parameter, it is useful to define a *strain rate mode parameter* n as follows:

$$n = \frac{\varphi\dot{\gamma}}{\psi\dot{e}}. \tag{10}$$ n

The parameter n assumes the following values for the corresponding loading modes:

1. $n = 0$ for isostatic pressing;
2. $n \to \infty$ for pure shear (p = 0);
3. $n = -\sqrt{6}$ for "free" forging;
4. $n = \sqrt{6}$ for drawing;
5. $n = \sqrt{\frac{2}{3}} sgn(\dot{\varepsilon_z})\frac{\varphi}{\psi}$ for constrained forging.

In the sequel, we shall consider cases 1, 3 and 5 only.
We refer to "free" forging as the loading mode represented in Fig. 1.a, a transverse compressive force acting at the top and bottom faces of the sample with no lateral confinement. Henceforth, the case of constrained forging, shown in figure 1.b, is nothing but an axial compression of the sample in a rigid die.

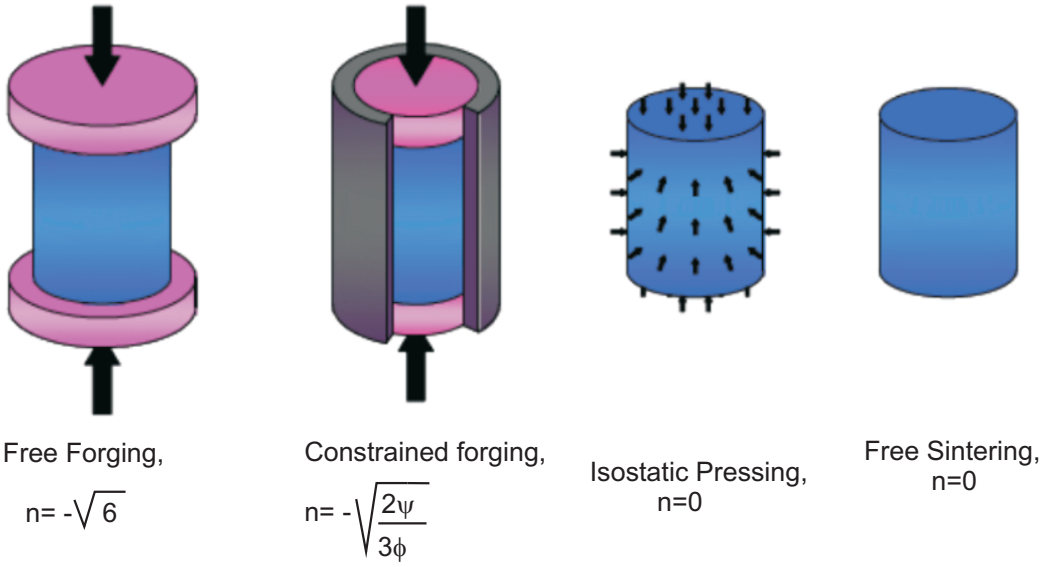

Figure 1: Different loading modes: forging, costrained forging, isostatic pressing, free sintering `modi`

From (1), (8) and (10), can be obtained the following relation:

$$\sigma_z = \frac{\sigma(w)}{w}\psi\dot{e}\Big[1+\sqrt{\frac{2}{3}}n\ sgn(\dot{\varepsilon}_z-\dot{\varepsilon}_r)\Big]+p_L-p_i; \qquad (11)$$ `sigma`

the dependence of effective equivalent stress $\sigma(w)$ on the effective equivalent strain rate w determines the constitutive behavior of a porous material.

Following Ashby [2], a power-law mechanism of deformation is assumed:

$$\frac{\sigma(w)}{\sigma_0} = A\Big(\frac{w}{\dot{\varepsilon}_0}\Big)^m, \qquad (12)$$ `Apowerlaw`

where A and m are material constants (A is temperature dependent, $0 < m < 1$), σ_0 and $\dot{\varepsilon}_0$ are the reference stress and the reference strain rate, respectively. Two limiting cases corresponding to ideal plasticity and linear viscosity are given by $m = 0$ and $m = 1$ respectively.
Equations (12) and (2) can be used to obtain an explicit expression for the ratio between the effective equivalent stress $\sigma(w)$ and the effective equivalent strain rate

w in terms of the porosity, the shear and bulk moduli, the loading mode and the shrinking rate:

$$\frac{\sigma(w)}{w} = \frac{\sigma_0 A}{\dot{\varepsilon}_0^m} w^{m-1} = \frac{\sigma_0 A}{\dot{\varepsilon}_0^m} |\dot{e}|^{m-1} \Big[\frac{\psi}{1-\theta} \Big(\frac{\psi}{\varphi} n^2 + 1 \Big) \Big]^{\frac{m-1}{2}}. \tag{13}$$

sigmaww

This paper is mainly devoted to study the influence of the interstitial pressure on the overall stress; for this reason, it is essential to monitor the magnitude $|\sigma_z - p_L|$ for each analyzed loading mode.

To this end, by substituting expression (13) into (11) the following relation can be obtain :

$$\sigma_z - p_L + p_i = \frac{A\sigma_0}{\dot{\varepsilon}_0^m} |\dot{e}|^m \Big[\frac{\psi}{1-\theta} (\frac{\psi}{\varphi} n^2 + 1) \Big]^{\frac{m-1}{2}} \Big[1 + \sqrt{\frac{2}{3}} n \; sgn(\dot{\varepsilon}_z - \dot{\varepsilon}_r) \Big]^{-\frac{1}{m}}. \tag{14}$$

sigma2

In order to achieve an analytical expression for the evolution of the material behavior during the sintering process, it is necessary now to introduce the porosity θ, defined as the ratio of the volume of pores and the total volume. By denoting the total volume of the sintered material as V_{tot} and the volume of the matrix and the one of the pores as V_{matrix} and $V_{pores} = V_{tot} - V_{matrix}$, respectively, the relative density can be written as:

$$\rho = \frac{V_{matrix}}{V_{tot}}. \tag{15}$$

The porosity reads:

$$\theta = \frac{V_{pores}}{V_{tot}} = 1 - \rho. \tag{16}$$

thetarho

Because of mass continuity and of the assumed incompressibility of the matrix (the shrinkage is only due to the change of the porosity) [18], the evolution law for the porosity is given by:

$$\dot{e} = \frac{\dot{\theta}}{1-\theta}. \tag{17}$$

etheta

Taking into account expression (17) and and reminding that the shrinkage is $\dot{e} < 0$ and thus $\dot{\theta} < 0$, relationship (14) leads to the following evolution equation for the porosity:

$$\dot{\theta} = sgn(\dot{\theta}) [sgn(\dot{\theta})(\sigma_z - p_L + p_i)]^{\frac{1}{m}} \frac{\dot{\varepsilon}_0}{(A\sigma_0)^{\frac{1}{m}}} \Big[\frac{\psi}{1-\theta} (\frac{\varphi}{\psi} n^2 + 1) \Big]^{\frac{1-m}{2m}} \Big[\psi \Big(1 + \sqrt{\frac{2}{3}} n sgn(\dot{\varepsilon}_z - \dot{\varepsilon}_r) \Big) \Big]^{-\frac{1}{m}} (1-\theta), \tag{18}$$

thetaP

which accounts for the contribution of the Laplace pressure and of the gas pressure in pores. The analog of (18) by neglecting such contributions was obtained by Olevsky and Molinari, [20] eq. 15.

IP

2.1. Evolution-law for the porosity for isostatic pressing processes

For the case of isostatic pressing, $\sigma_z = \sigma_r$ and in the sequel their common value will be denoted by σ. Furthermore, here the loading mode parameter n is zero and the process antails a monotonically decrease of the porosity, i.e. $\dot{\theta} < 0$; hence, relation (18) reduces to the following expression:

$$\dot{\theta} = -[-(\sigma - p_L + p_i)]^{\frac{1}{m}} \frac{\dot{\varepsilon}_0}{(A\sigma_0)^{\frac{1}{m}}} (1-\theta)^{\frac{3m-1}{2m}} \psi^{\frac{-(1+m)}{2m}}. \tag{19}$$

thetaPIP

Obviously, since $\dot{\gamma} = 0$, the shear modulus φ, has no influence on the process. The bulk modulus ψ is a known function of the porosity θ; for such a function, here and further, we shall use the expressions given in section 2.1.
Let us notice that, for this case, Mc Meeking's and Castaneda's models give the same behavior. This is because of the expression of the bulk modulus ψ, which is indeed the same for both models.

Eq. (19) may be normalized by using the dimensionless specific time defined as follows:

$$\tau_L = \left[\frac{p_{l0}}{\sigma_0 A}\right]^{\frac{1}{m}} \dot{\varepsilon}_0, \tag{20}$$ tauL

so that the evolution law for the porosity (19) can be rewritten as:

$$\frac{\partial \theta}{\partial \tau_L} = -(1-\theta)^{\frac{3m-1}{2m}} [-(\sigma - p_L + p_i)]^{\frac{1}{m}} \psi^{\frac{-(1+m)}{2m}} \tag{21}$$ thetaPIPadim

For further developments, it is useful to introduce a dimensionless pressure parameter, called Specific External Pressure (S.E.P.) and defined as follows:

$$S.E.P. = \frac{\sigma}{\alpha / r_0}, \tag{22}$$ SEP

where α denotes the surface tension and r_0 the averaged radius of the particles (for further explanation, see Sect. 2.3).

subsec:2.1

2.2. Dependence of the shear and bulk moduli on the porosity

In the literature several studies relative to the determination of the bulk and shear moduli are present.
In particular we shall use four different models:

- $\begin{cases} \varphi = (1-\theta)^2 \\ \psi = \frac{2}{3}\frac{(1-\theta)^3}{\theta} \end{cases}$ Skorohod model [26];
- $\begin{cases} \varphi = \frac{(1-\theta)^{\frac{2}{1+m}}}{1+\frac{2}{3}\theta} \\ \psi = \frac{2}{3}\left(\frac{1-\theta^m}{m\theta^m}\right)^{\frac{2}{m+1}} \end{cases}$ Duva Castaneda-Duva-Crow model [22, 7];
- $\begin{cases} \varphi = \left(\frac{1-\theta}{1+\theta}\right)^{\frac{2}{1+m}} \\ \psi = \frac{2}{3}\left(\frac{1-\theta^m}{m\theta^m}\right)^{\frac{2}{m+1}} \end{cases}$ Mc Meeking-Sofronis model [27];
- $\begin{cases} \varphi = \frac{(1-\theta)^{\frac{2}{1+m}}}{1+\frac{2}{3}\theta} \\ \psi = \frac{m+1}{3}\frac{(1+\theta)(1-\theta)^{\frac{2}{m+1}}}{\theta} \end{cases}$ Cocks model [5].

In figures 2 and 3 moduli ψ and φ are plotted as functions of the porosity for different values of the parameter m.
The model delivered by Skorohod account for linear-viscous incompressible material with voids only: indeed the moduli ψ e φ are independent from the parameter m.

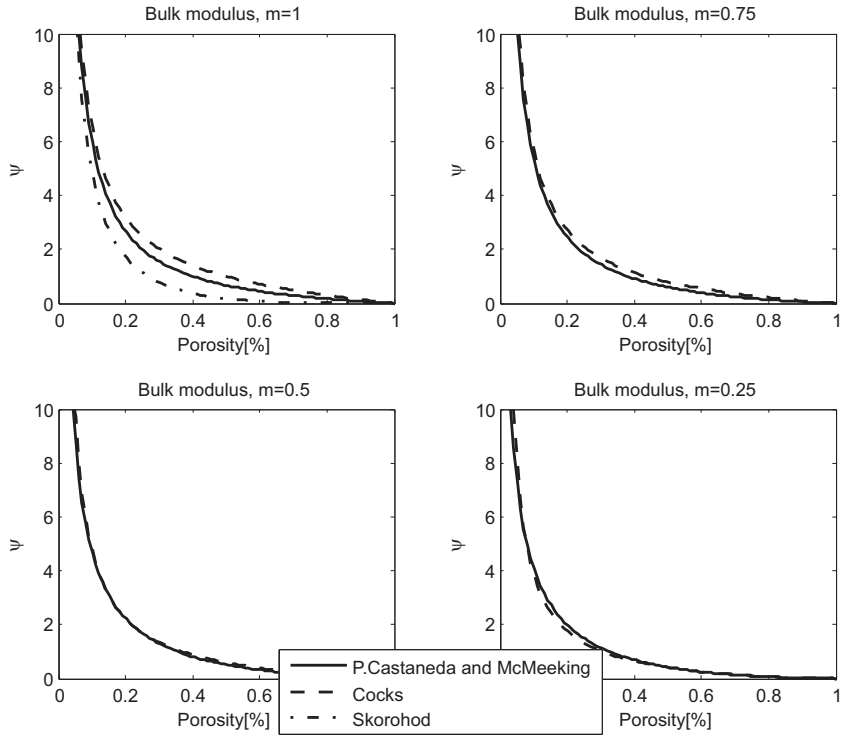

Figure 2: Bulk modulus ψ as function of porosity, for different values of the strain rate sensitivity m.

psi

laplace

2.3. Dependence of the Laplace pressure on the porosity

The effective Laplace pressure p_L is the result of collective action of local capillary stresses in a porous material. A variety of approaches can be found in the literature. We shall consider two possible derivations of the expression for the Laplace pressure.

1. *Sintering stress derived by using a stochastic approach*
   This derivation was employed by Skorohod [26], who obtained p_L by calculating the surface free energy per unit mass with respect to the specific volume of the porous material by assuming spherical particles. The achieved result may be stated as follows:

$$p_L = p_{l0}(1-\theta)^2 = \frac{3\alpha}{r_0}(1-\theta)^2, \tag{23}$$

   p_L2

   where α is the surface tension and r_0 is the characteristic radius of particles.

2. *Sintering stress derived by averaging of the dissipation*
   Here we summarize results shown in [19], Appendix A.2.2, about the derivation of an expression for the Laplace pressure. A hollowed sphere is considered as a schematic for a pore (see Figure 4); at its surface, namely for ($r = R_1$), the pressure $p_{l0} = \frac{2\alpha}{r_0}$ is applied, whereas the external boundary ($r = R_2$) is stress

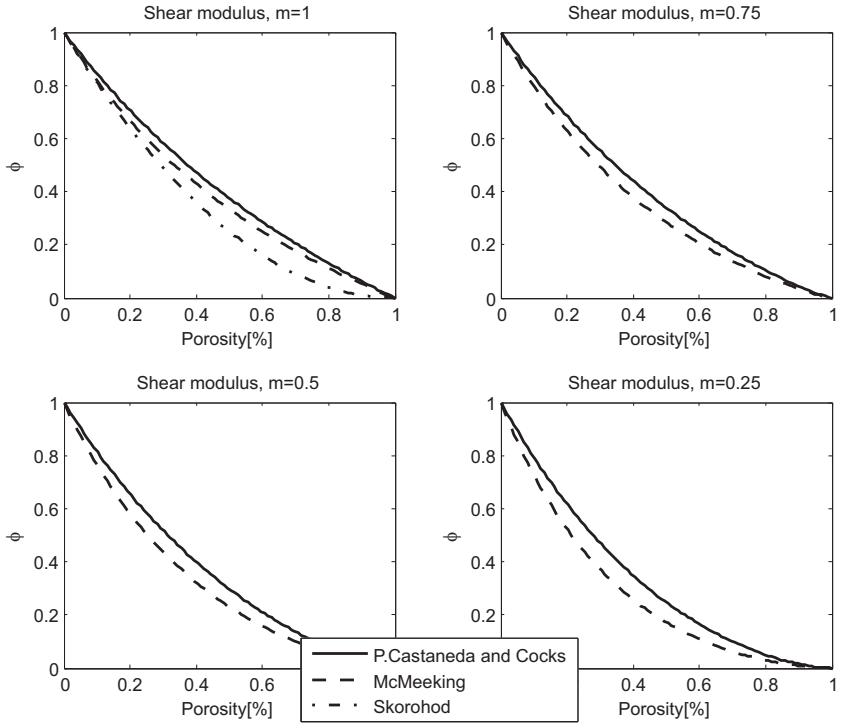

Figure 3: Shear modulus φ as function of porosity, for different values of the strain rate sensitivity m. phi

free (where r denotes the radial coordinate).
The porosity is then determined by the volume fraction:

$$\theta = \left(\frac{R_1}{R_2}\right)^3. \tag{24}$$ poro1

The introduction of standard compatibility conditions into the constitutive relation (1) yields the radial and circumferential stresses as functions of the unknown radial velocity $V_r(r)$ (and of p_L). Finally, the stress balance (in the radial direction) allows for determining:

$$V_r(r) = -\frac{p_{l0} R_1^3 R_2^3}{2\frac{A\sigma_0}{\dot{\varepsilon}_0^m}\varphi(R_2^3 - R_1^3)r^2}, \tag{25}$$ V

for $m = 1$, namely in the case of linearly-viscous behavior.
Henceforth, the effective equivalent strain rate w (see (2)) appearing in (1), is relevant for the expression of the dissipation potential proposed in [18], eqn.(26), i.e.:

$$D = \frac{\frac{A\sigma_0}{\dot{\varepsilon}_0^{-\frac{1}{m}}}}{m+1}(1-\theta)w^{m+1}. \tag{26}$$ diss

Through the latter expression, the dissipation of the matrix and its average on the volume of the hollowed sphere may be deduced.

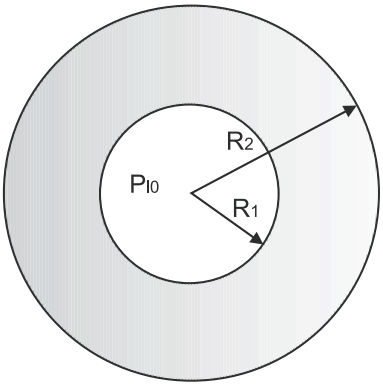

Figure 4: A representative element of porous medium

poro

On the other hand, the dissipation of the effective porous material, subject to free sintering, is evaluated; its connection with the volume averaged dissipation through the Hill's identity ([19], eqn. A29) allows for determining the following expression for the Laplace pressure:

$$p_L = \frac{2\alpha}{r_0}\sqrt{\frac{3}{2}\psi(\theta)\frac{\theta}{1-\theta}}. \tag{27}$$

Pl1

The latter can be particularized to obtain the sintering stress associated to the models cited above; in particular we get:

- $p_L = \frac{2\alpha}{r_0}(1-\theta)$ for the Skorohod model,
- $p_L = \frac{2\alpha}{r_0}$ for the Castaneda and Mc Meeking models,
- $p_L = \frac{2\alpha}{r_0}\sqrt{1+\theta}$ for the Cocks model.

Figure 5 shows the dependence of the Laplace pressure on the porosity θ.
The stochastic approach, yielding relation (23), gives a parabolic trend of the Laplace pressure. This is increasing when the porosity decreases and it is independent on the value of the parameter m, so that p_L does not depend upon the material behavior. In particular, the values of pressure calculated through (27) are compatible enough with the ones obtained by (23) in the range of interest of porosity for common sintered components (see the blow-up shown in fig. 5).

gaspressure

2.4. Gas pressure in pores and its dependence upon the porosity

During the sintering process, the porosity becomes isolated and the final stage of sintering starts at a relative density $\rho = 90\%$, i.e. at the closure porosity $\theta_c = 0,1$. At this time, the gas pressure in pores is equal to the external pressure.; as the relative density ρ increases, the gas pressure in closed pores also increases. The more natural way to account for such a phenomenon is through the ideal gas law (see [33, 3]), i.e. $(p_i + p_{atm})V_{pores} = const$, where p_i is the gas pressure in the pores and p_{atm} the atmospherical pressure.
Reminding that, thanks to the incompressibility of the matrix, $V_{matrix} = const$ during

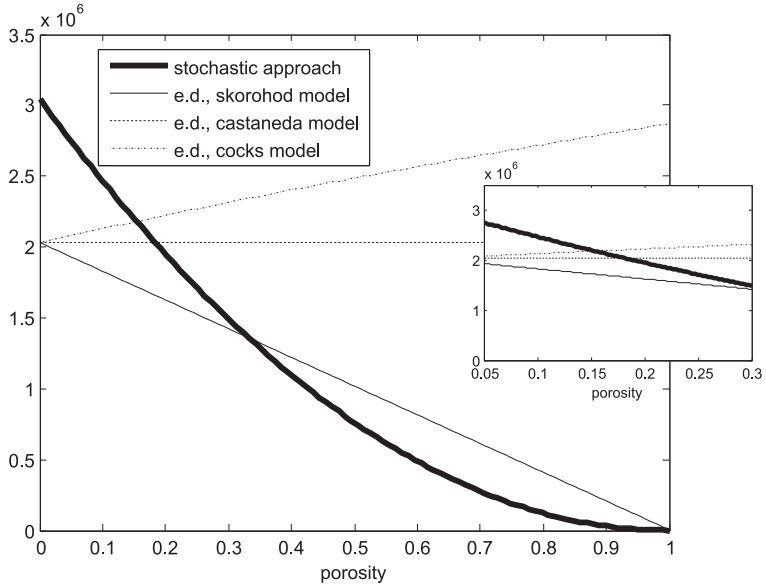

Figure 5: the Laplace pressure as function of porosity

figurePl

the process, from ideal gas law it follows that the quantity $(p_i + p_{atm})\frac{1-\rho}{\rho} = (p_i + p_{atm})\frac{V_{pores}}{V_{matrix}}$ remains constant. Recalling (16), the relationship can be rewritten as:

$$(p_i + p_{atm})\frac{\theta}{1-\theta} = const = (p_0 + p_{atm})\frac{\theta_c}{1-\theta_c}, \tag{28}$$

where p_0 is the external pressure (i.e. the gas pressure in the pores when the porosity closes).
Thus, the evolution of the pressure in the pores during sintering process is given by:

$$p_i = \begin{cases} 0 \quad if\ \theta > \theta_c \\ (p_0 + p_{atm})\frac{\theta_c}{\theta}\frac{1-\theta}{1-\theta_c} - p_{atm} \quad if\ \theta < \theta_c \end{cases} \tag{29}$$

pi

It is noticeable that, in the case of isostatic pressing, the external pressure is equal to the applied stress $|\sigma|$.

The effect of the Laplace pressure p_L and of the gas pressure in pores p_i are investigated in Sect. 3 and 4, respectively.

3. Effect of the Laplace pressure on sintering processes entailing isostatic-pressing

Laplaceeffect

In the present section, the effect of the Laplace Pressure on sintering processes entailing isostatic-pressing is studied. To be precise, processes entailing, as driving force, only the stress due to the external load are compared to process in which the Laplace pressure are taken into account.

Figure 6 shows the time evolution of the porosity during an isostatic pressing process that reduce the porosity from 30% to 5%, obtained by using the Castaneda-Duva-Crow model for $S.E.P. = 10$, in two cases:

- accounting for the sintering stress (continuous line), the driving force of the process is $\sigma - p_L$;
- neglecting the interstitial pressure (dashed line), the driving force is the stress due to the external load, σ.

The latter describes the approximation adopted in [20]. Indeed, since $|\sigma - pl| > |\sigma|$, the time decay of the porosity would be lower than the real one. Nevertheless, we record that the time evolution of the porosity has a qualitative analog to the one obtained by neglecting p_L (see Figure 6).
When the strain rate sensitivity m decreases, the initial part of both graphs become steeper. Indeed, for infinite slope, the material behavior would be perfectly plastic (this would correspond to $m = 0$).

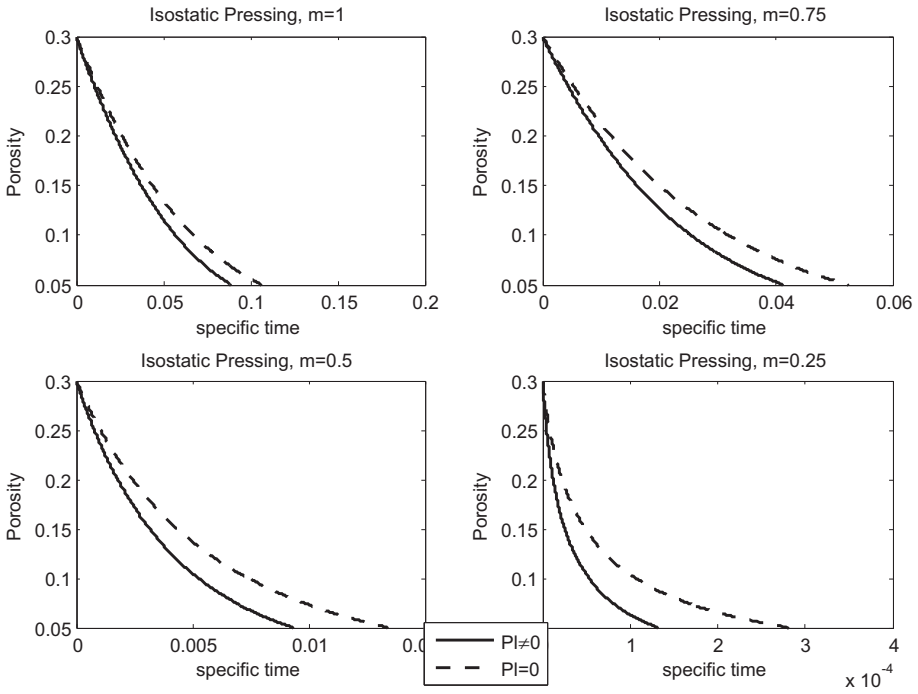

Figure 6: ISOSTATIC PRESSING-Evolution of Porosity for S.E.P.=10 IP1

Moreover, it can be noticeable that the gap between the two curves is higher for lower values of the strain rate sensitivity m, hence the Laplace pressure has more influence on the sintering process when the material tends towards the plastic behavior. This may be explained by the (Ashby) power-law (eq. (12)) relating the equivalent strain rate w and the effective equivalent stress $\sigma(w)$. Indeed, equation (12), displayed in Figure 7, indicates that for lower values of the parameter m, the effective equivalent strain rate is more sensitive to stress changes; in particular, for such values, it is displayed the significant change of w by considering as driving force $|\sigma - p_L|$ instead of $|\sigma|$.

Figure 8 is the analog of 6 for lower value of external pressure, i.e. $S.E.P. = 1$. Here, the gap between the curves is remarkable because, in this case, the "driving

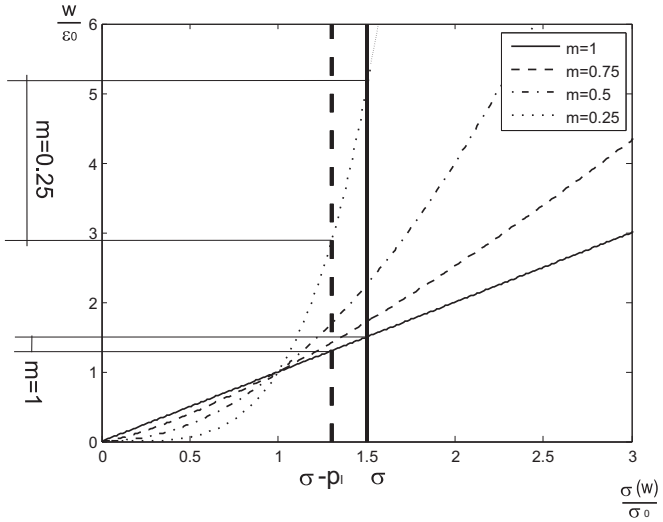

Figure 7: (Ashby) power law: sensitivity of the effective equivalent strain rate to the variation between σ and $|\sigma - p_L|$.

powerlaw

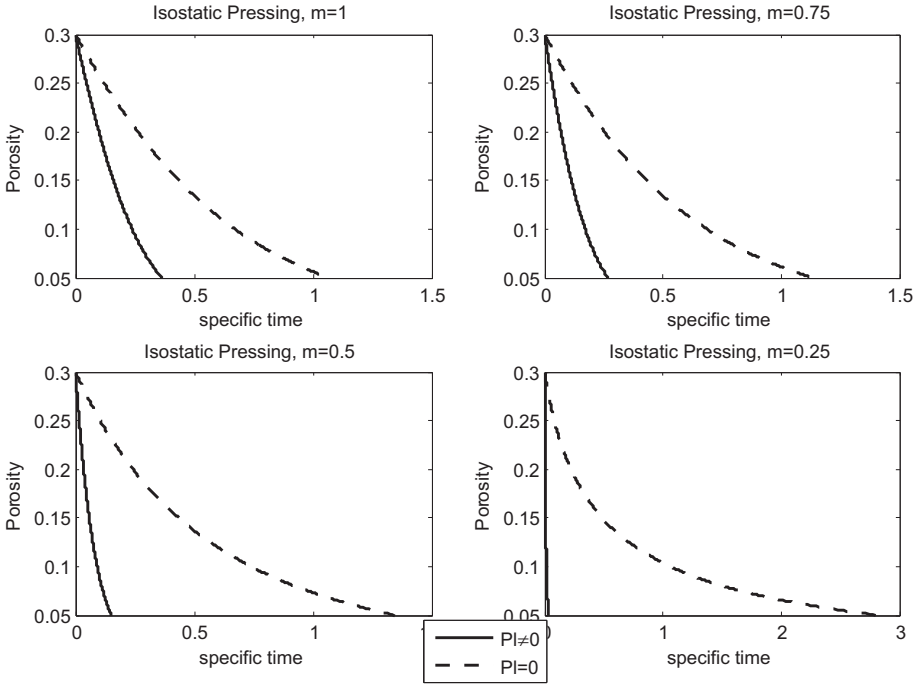

Figure 8: ISOSTATIC PRESSING-Evolution of Porosity for S.E.P.=1

IP3

sintering force" is basically the Laplace pressure, simply because it is higher than the externally imposed stress.

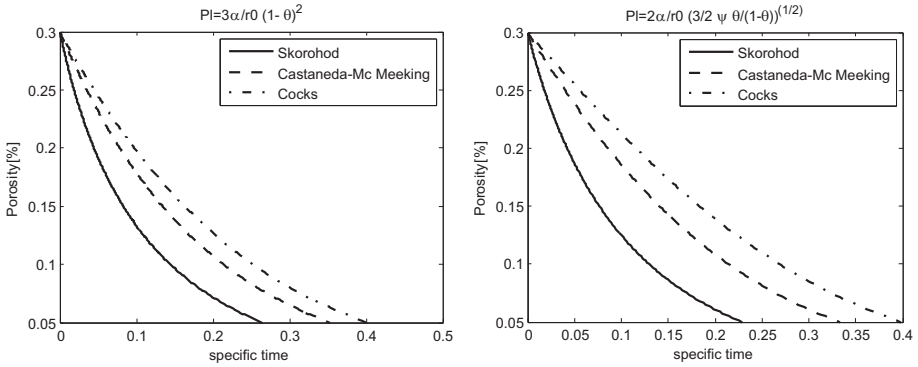

Figure 9: ISOSTATIC PRESSING-Evolution of Porosity for S.E.P.=5 ,m=1, for different models

IP4

A comparison among the three different models for the shear and bulk moduli φ ad ψ and between the two different expressions for p_L (see (23) e (27)) is performed in the sequel. Figure 9 shows such a comparison for S.E.P.=5 and for a material with linear-viscous behavior (m=1).

Time-evolution diagrams shown by figures 9.a and 9.b are similar, because the value of the Laplace pressure given by equations (23) e (27) are compatible enough for porosities between 30% and 5% (see the blow-up in Figure 5). The differences among curves relative to the various considered models are due to the corresponding expressions of the bulk modulus ψ.

3.1. Influence of the interstitial stress on industrial processes entailing isostatic pressing

indIP

A specific metallic alloy (aluminum-zinc-magnesium-copper alloy) is examined in this section. This is motivated by its extended use in industrial sintering processes. The main features of this material are listed in table 1:

For aluminum alloys, the averaged sintering time is thirty minutes and usually the applied external pressure is of the order of $100MPa$ [16, 24, 8].
It may be shown that the important parameters influencing the Laplace pressure are the radius of the grains r_0 and the surface tension α.
Values of powder grain size from 50 nm to 50 μm are here taken into account.

In the sequel, we shall examine the discrepancies on the estimate of the sintering times evaluated by either neglecting or accounting for the sintering stress p_L. Furthermore, we shall also calculate the residual porosity in both of the cases mentioned above.

Young's modulus	E	70,7	GPa
Poisson's ratio	υ	0,325	
surface tension	α	1,128	N/m
activation energy	Q	14390	kJ
melting temperature	T_m	659	°C
average radius of the particles	r_0	5-50	μm
sintering temperature	T_s	100-350	°C
sintering pressure	P_b	600-610	Mpa

Table 1: Characteristics of the considered aluminum-zinc-magnesium-copper alloy

tab1

indIP1

3.1.1. Threshold external loading pressures and sintering times

Here, we are interested to compare the sintering times t and t_0 employed to reduce the porosity from 30% to 5% in cases in which the "sintering driving force" is taken to be either $|\sigma - p_L|$ or $|\sigma|$ respectively. We are also interested into calculating the values of the external pressure p^* for which the discrepancy between the sintering times, i.e. $\frac{t-t_0}{t}$, attains the values 5%, 10% and 15% respectively. Obviously, whenever the external pressure is less than p^*, for the given value of discrepancy, for example 5%, an error greater than 5% occurs by neglecting the effect of the Laplace pressure.

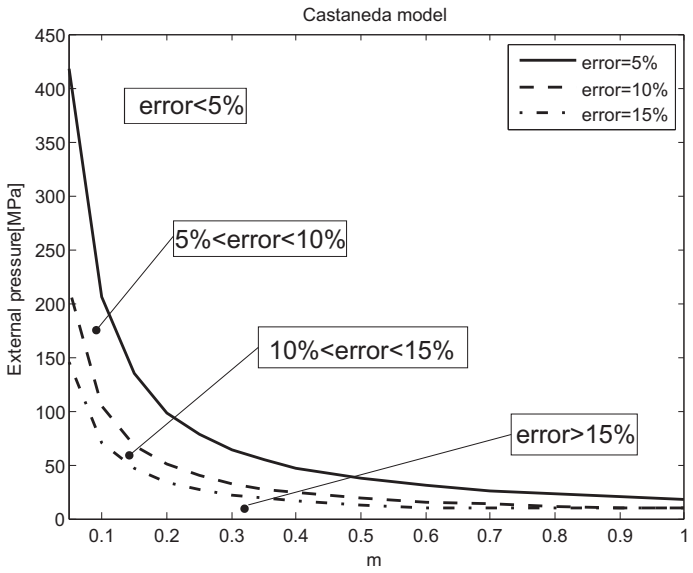

Figure 10: Threshold pressure p^*, for $5\mu m$ powder

IPpressureCastaneda

In Figure 10 and 11 are shown the threshold pressures for $5\mu m$ and $50nm$ pow-

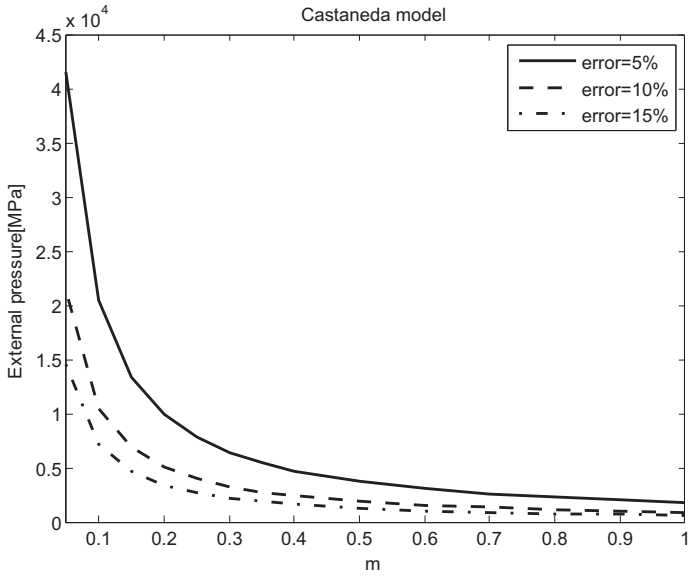

Figure 11: Threshold pressure p^*, for $50nm$ powder

IPpressureCastanedaNANO

ders (obtained by the model of Castaneda). It is immediate to note that the effect of the Laplace pressure becomes more relevant for lower values of the powder grain size. Henceforth, in this case the threshold pressures are considerably high.
The comparison between threshold pressures obtained by using the Castaneda and Cocks models shows that they do not exhibit meaningful differences.

The result of these sections rely upon the model for the Laplace pressure based on the stochastic approach (equation (23), discussed in section 2.3). Instead, equation (27), derived by averaging of the dissipation, does not allow for evaluating p_L for different values of the strain rate sensitivity parameter m. However, the values of the threshold pressure obtained by using the latter model are in complete agreement with the ones obtained by using the former.

indIP2

3.1.2. Residual porosity

The residual porosity is a fundamental feature of the actual material, because, among others, determines the mechanical properties of a sintered specimen.
A thirty minutes sintering process with external loading pressure of $100MPa$ is now considered. Here, we are interested to compare the residual porosities θ_r and θ_{r0} after thirty minutes, wherever the "sintering driving force" is taken to be either:

- $|\sigma - p_L|$ or
- $|\sigma|$,

respectively.
For the different values of powder grain size mentioned above, we are able to calculate the value of the strain rate sensitivity m that permits to have a sintering reference time of the order of thirty minutes 30'. For the sake of convenience, without loss of

generality, in the sequel a time range corresponding to a variation of $\pm 30\%$ of the reference time is considered.
Figure 12 shows the sintering time as a function of m and highlights the values of strain rate sensitivities m corresponding to the real sintering times.

With such values of the parameter m, we may calculate the error

$$e = \frac{\theta_r - \theta_{r0}}{\theta_r}, \tag{30}$$

errore

occurring wherever the Laplace pressure p_L is neglected. Figure 13 shows values of such an error as a function of the strain rate sensitivity m, for grain sizes between $100nm$ and $5\mu m$.

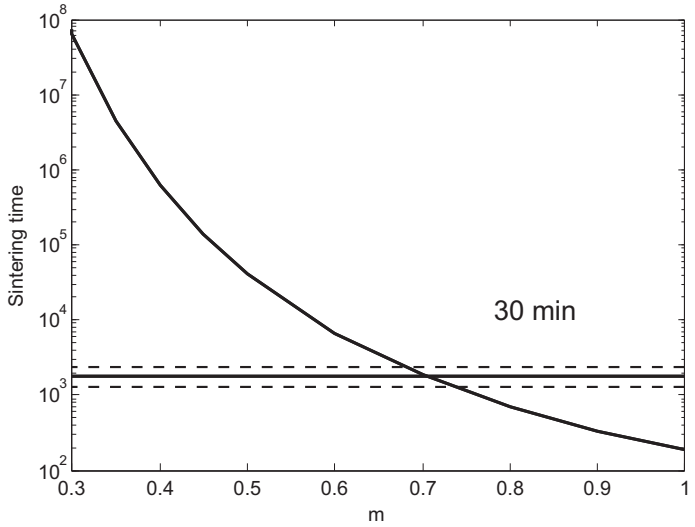

Figure 12: Sintering time as a function of the strain rate sensitivity m

tempiM

It is immediate to note that, for nano powders (i.e. for grain size less than $1\mu m$) the error becomes much higher than in the case of micro powders. In particular, for sizes of the order of $100nm$ an error of about 40% may occur, while for $20nm$ the error is even of the order of 80% (not shown in figure 13. For lower grain sizes, the gap between θ_r and θ_{r0} is higher than the previous cases.

The second parameter influencing the Laplace pressure is the surface tension α; there are lots of uncertainties on the determination of its value [12]. Hence, because of lack of reliability, the sensitivity of the model to variations of α in the range $\pm 50\%$ is analyzed.
Figure 14 shows the error e (defined by (30)) as a function of the surface tension α, for different values of the powder grain size.
For increasing values of α, the Laplace pressure grows and hence the gap between θ_r and θ_{r0} increases accordingly; this phenomenon turns out to be more relevant for lower powder grain sizes.

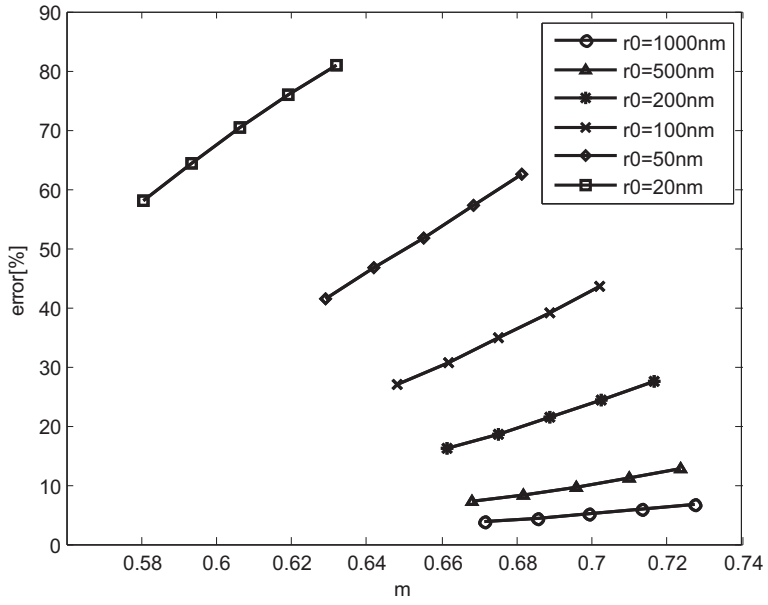

Figure 13: Errors $e\%$ on the residual porosity for different values of the grain size r_0 ITETAerroreIP

4. Effect of the gas pressure in pores on sintering processes entailing isostatic-pressing

gaspressureeffect

In the present section, the effect of the gas pressure in the pores on sintering processes entailing isostatic-pressing is studied through the comparison between results obtained by accounting for p_i and by neglecting it. Isostatic pressing processes that reduce the porosity from 30% to 5% are considered.
The evolution of the pressure in the pores during sintering process is given by (29) where, in the case of isostatic pressing, the external pressure p_0 is equal to the absolute value of the applied stress $|\sigma|$.
Figure 15 shows, for $S.E.P. = 10$, the absolute values of the stress due to the external load, the gas pressure in the pores and the Laplace pressure.

Figure 16 shows the values of the total driving force, for different values of $S.E.P.$, in two cases:

- accounting for the whole driving force (dashed line) $\sigma - p_L + p_i$;
- neglecting the gas pressure in the pores (dotted line), i.e. the driving force is considered to be $\sigma - p_L$.

The latter describes non-pressurized pores. Indeed, since no pressure could act against stresses caused by external loading (and Laplace pressure), the time decay of the porosity, in this case, would be faster than the real one. It is noticeable that, since $\sigma - p_L < 0$ and $p_i \geq 0$ during the whole sintering process (see equation (29)), the total driving force $\sigma - p_L + p_i$ may turn out to become null at a definite value of porosity. Such a value will be denoted by θ^* and it is given by the following condition:

$$|\sigma - p_L(\theta^*)| = p_i(\theta^*). \tag{31}$$

thetastar

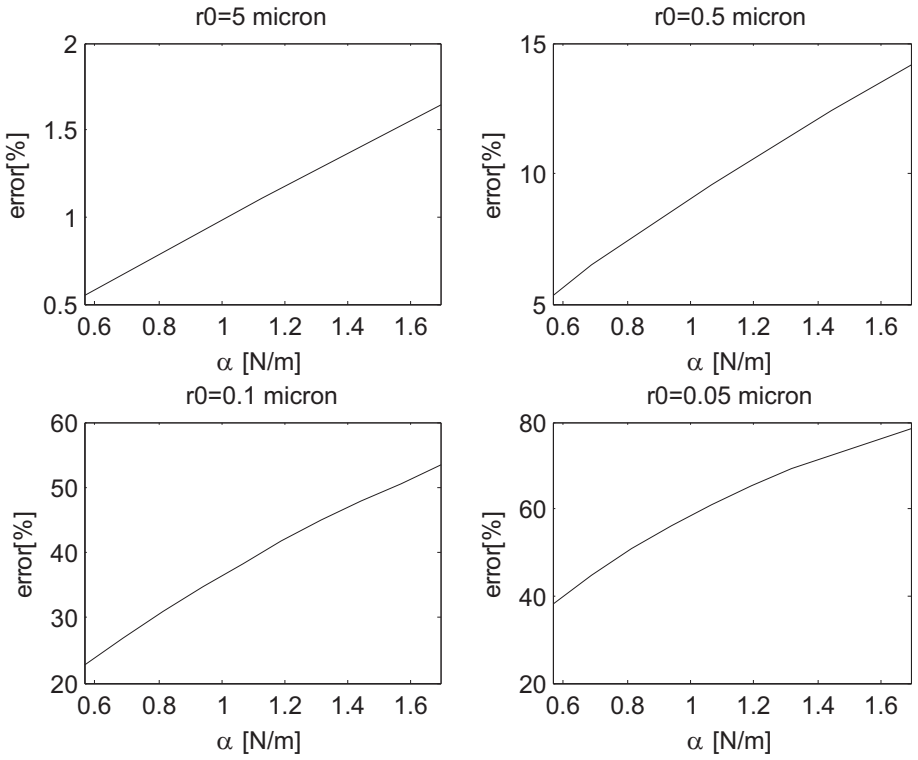

Figure 14: Errors $e\%$ on the residual porosity, for different values of the surface tension α IPvarioALPHA

In the limiting case for which condition (31), equation (21) yields $\dot{\theta} = 0$ and hence $\theta = const.$ Thus, whenever such condition is achieve the porosity remains constant at the limit value θ^*.
It is evident that the value of θ^* depends upon the external load and on the choice of expression (23) or (27) for the Laplace pressure. Moreover, since $p_i = 0$ for $\theta > \theta_c$, that condition (31) can be verified only in the third phase of sintering, when $p_i > 0$; it leads to $\theta^* < \theta_c$.

By denoting by θ_F the desired porosity at the end of the process and recalling that θ_c denotes the closure porosity, i.e. the value of the porosity for which the pores becomes isolated, we may now distinguish two cases:

- *Case in which* $\theta_F < \theta^* < \theta_c$.
  Figure 17 shows the time evolution of the porosity, obtained by using the Castaneda-Duva-Crow model, for different values of the strain rate sensitivity m, for $S.E.P. = 10$, in two cases:
  - accounting for the gas pressure in the pores p_i (continuous line);
  - neglecting it (dashed line).

  It is evident that, since $\theta > \theta_c$ (i.e. during first and second phase of sintering), the evolution of the porosity obviously is not affect by the presence of p_i and hence the curves coincide. When the third phase begins, at porosity $\theta = \theta_c$, the

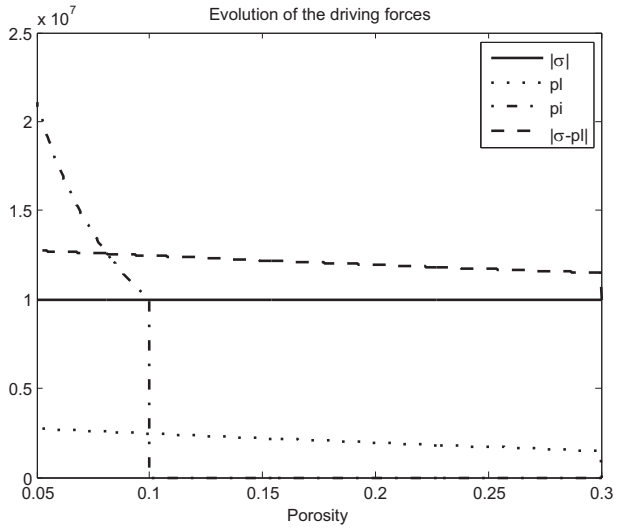

Figure 15: Dimensionless sintering driving forces

drivingforces

dashed line moves away from the continuous one; as stated above, the sintering time obtained by accounting for the gas pressure in pores is higher than the one obtained by neglecting it.
The fundamental result, in the case under exam, is that the desired final value of the porosity θ_F can not be obtained; the value of the porosity at the end of the process is given by $\theta^* > \theta_F$. Moreover, since whenever the condition (31) is achieve the rate of change of the porosity goes to zero; in proximity of such a condition, the time-porosity graph presents an horizontal plateaux. It leads to a stretch of sintering times, as it is evident from figure 17.

- *Case in which* $\theta^* < \theta_F$.
  Figure 18 shows the time evolution of the porosity, obtained by using the Castaneda-Duva-Crow model, for different values of the strain rate sensitivity m, for $S.E.P. = 1$. It is evident from figure 16 that, for such a value of $S.E.P.$, the critical porosity θ^* is not achieve in the range of considered porosity, i.e. $\theta^* < \theta_F$. This allow to obtain, at the end of the process, the desired porosity θ_F. The unique effect of the gas pressure in the pores is to stretch the sintering times. Such a phenomenon will be studied in the following subsection.

In both cases, the gap between the two curves is higher for lower values of the strain rate sensitivity m, hence the presence of gas pressure in the pores has more influence on the sintering process whenever the material tends towards the plastic behavior. this may be explained by the (Ashby) power-law (eq. (12)), that indicates that for lower values of the parameter m, the effective equivalent strain rate is more sensitive to stress changes.

A comparison among the three different models for the shear and bulk moduli φ ad ψ and between the two different expressions for p_L (see (23) e (27)) is performed

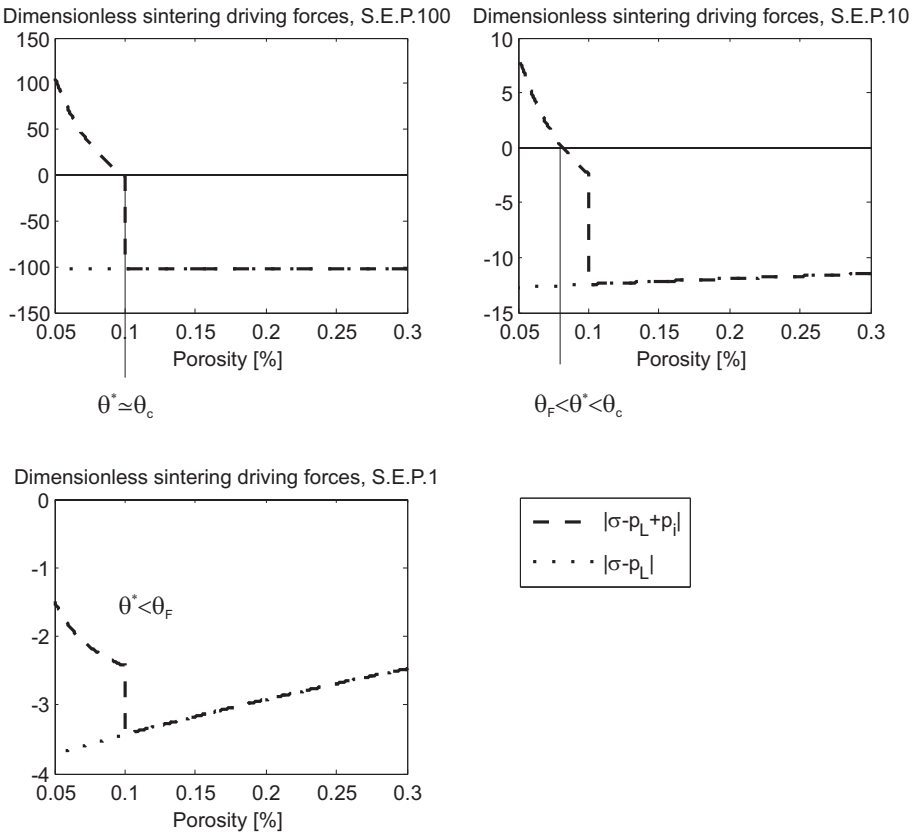

Figure 16: Dimensionless total sintering driving forces

`drivingforces2`

in the sequel. Figure 19 shows such a comparison for $S.E.P. = 1$ and for a material with linear-viscous behavior ($m = 1$).

Time-evolution diagrams shown by figures 19.a and 19.b are quite similar, because the value of the Laplace pressure given by equations (23) e (27) are compatible enough for porosities between 30% and 5% (see the blow-up in Figure 5). The differences among curves relative to the various considered models are due to the corresponding expressions of the bulk modulus ψ.

Figure 20 shows such a comparison for $S.E.P. = 10$, for $m = 1$.

Also in this case, diagrams shown by figures 20.a and 20.b are similar. The differences among curves relative to the various considered models are due to the corresponding expressions of the bulk modulus ψ, leading, in the case of $p_L = \frac{2\alpha}{r_0}\sqrt{\frac{3}{2}\psi(\theta)\frac{\theta}{1-\theta}}$ to slightly different values of the critical porosity θ^*.

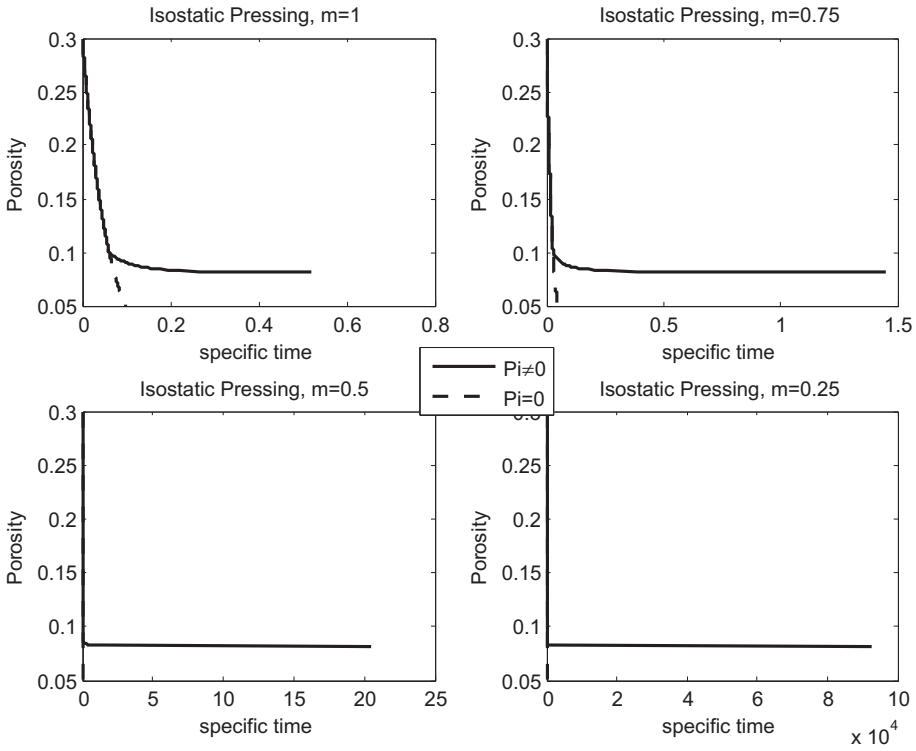

Figure 17: ISOSTATIC PRESSING-Evolution of Porosity for S.E.P.=10

pi10

4.1. Influence of the interstitial stress on industrial processes entailing isostatic pressing

indIP_PI

In analogy to the analysis performed in 3.1, we are interested in determine if it is exists a threshold for the external pressure under (or over) which the effect of the gas pressure in pores is negligible in a "real" industrial process. The aluminum-zinc-magnesium-copper alloy presented in section is here considered.

As discussed above, in the case of isostatic pressing, the gas pressure in the pores at the beginning of the third phase of sintering (i.e. at the closure porosity θ_c) is equal to the external pressure. Hence, whenever the external pressure increases, also the pressure in the pores increases, acting "against" the sintering process and allowing to not reaching the desired final porosity. Figure 21 show the final porosity that can be reached as a function of the applied external pressure, for different values of the strain rate sensitivity m, for $5\mu m$ and $50nm$ powders, respectively.

Since the required final porosity can be reached only for low values of the external pressure (and, hence, of the gas pressure in pores), it has no sense to look for an external pressure threshold under which the effect of the gas pressure in pores is negligible from the point of view of the sintering time, or the error on the evaluation of the residual porosity, in analogy to 3.1.1 and 3.1.2.

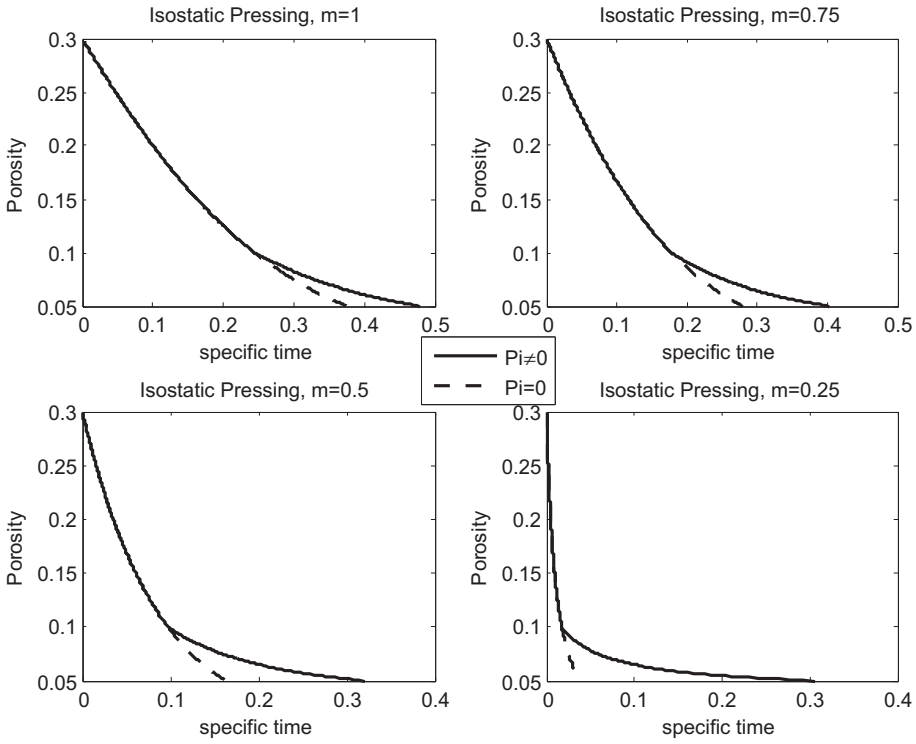

Figure 18: ISOSTATIC PRESSING-Evolution of Porosity for S.E.P.=1

pi1

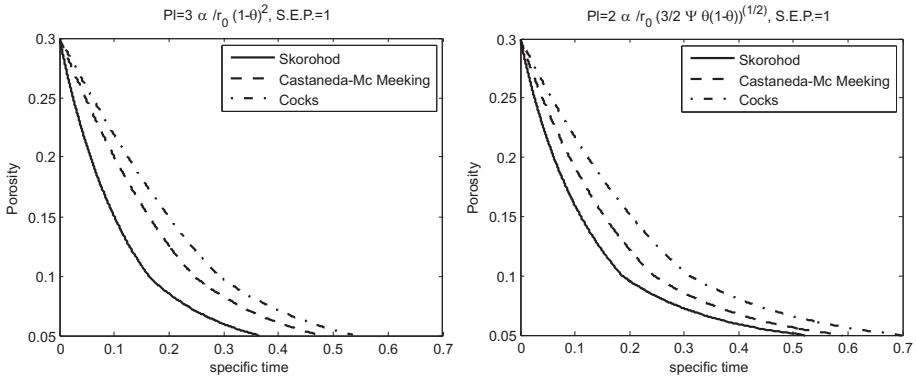

Figure 19: ISOSTATIC PRESSING-Evolution of Porosity for S.E.P.=1

PIconfronto1

5. Stability

stabIP

lowerstabIP

5.1. Lower order analysis

Here we may denote by $\theta^{(0)}(t)$ the fundamental solution of the evolution law (19) associated with an uniform distribution of the initial porosity. Following [20], Sect.

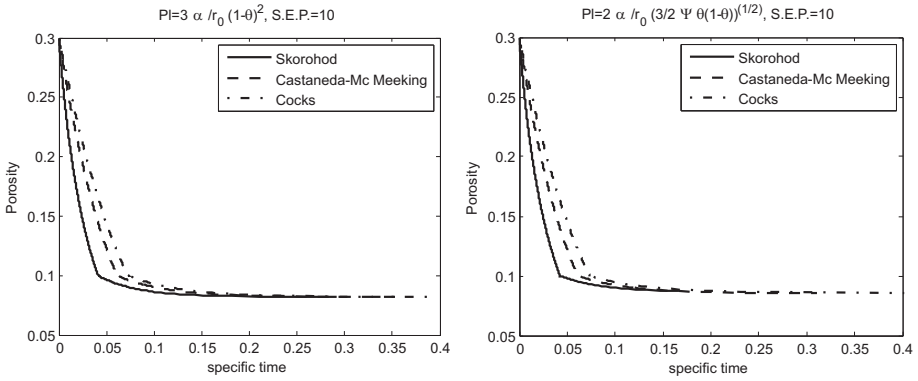

Figure 20: ISOSTATIC PRESSING-Evolution of Porosity for S.E.P.=1

PIconfronto10

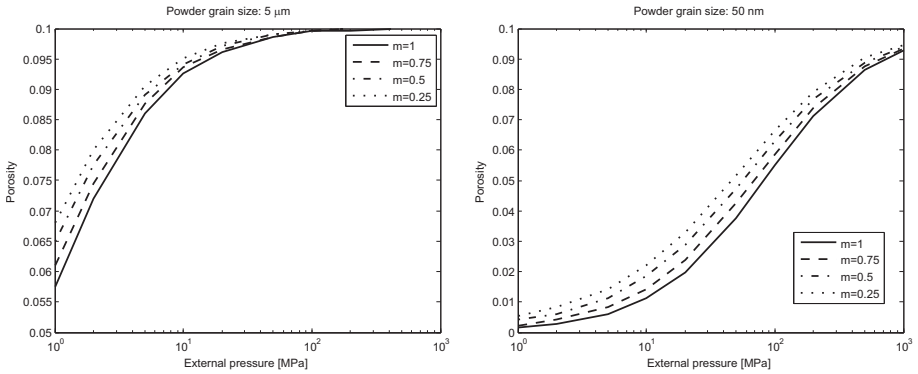

Figure 21: Final porosity as a function of applied external pressure, for $5\mu m$ powder

porFINALE

3.1.1, we assume that the perturbed solution has the form

$$\theta(t) = \theta^{(0)}(t) + \delta\theta(t)\exp(\lambda(t - t_0)), \tag{32}$$

where the magnitude of the perturbation $\delta\theta(t)$ is taken to be much smaller than the one of $\theta^{(0)}(t)$ at all times. In [20], section 3.1.1, a normalized perturbation growth rate with respect to the current rate of change of porosity is considered; this is done in order to have a "first" order information about the stability of the process.
The quantity $\lambda = \frac{\delta\dot{\theta}}{\delta\theta}$ can be regarded as the perturbation growth rate. It is possible to calculate the quantity $\frac{\lambda}{\dot{\theta}}$ as a function of θ, θ_0, m, p_L and the external pressure. This can be done in the framework of the three different models considered in the previous sections.

Because, during sintering, shrinkage occurs monotonically ($\dot{\theta} \leq 0$), the problem is linearly stable if $\lambda < 0$, i.e. $\frac{\lambda}{\dot{\theta}} > 0$, whereas linearly unstable if $\lambda > 0$, that is $\frac{\lambda}{\dot{\theta}} < 0$.
In figure 22 the quantity $\frac{\lambda}{\dot{\theta}}\delta\theta$ is plotted as a function of θ, for different values of the strain rate sensitivity m, for $S.E.P. = 10$. It is evident from the graph that the process is always linearly stable. The value of the applied external pressure does not change

the stability condition.

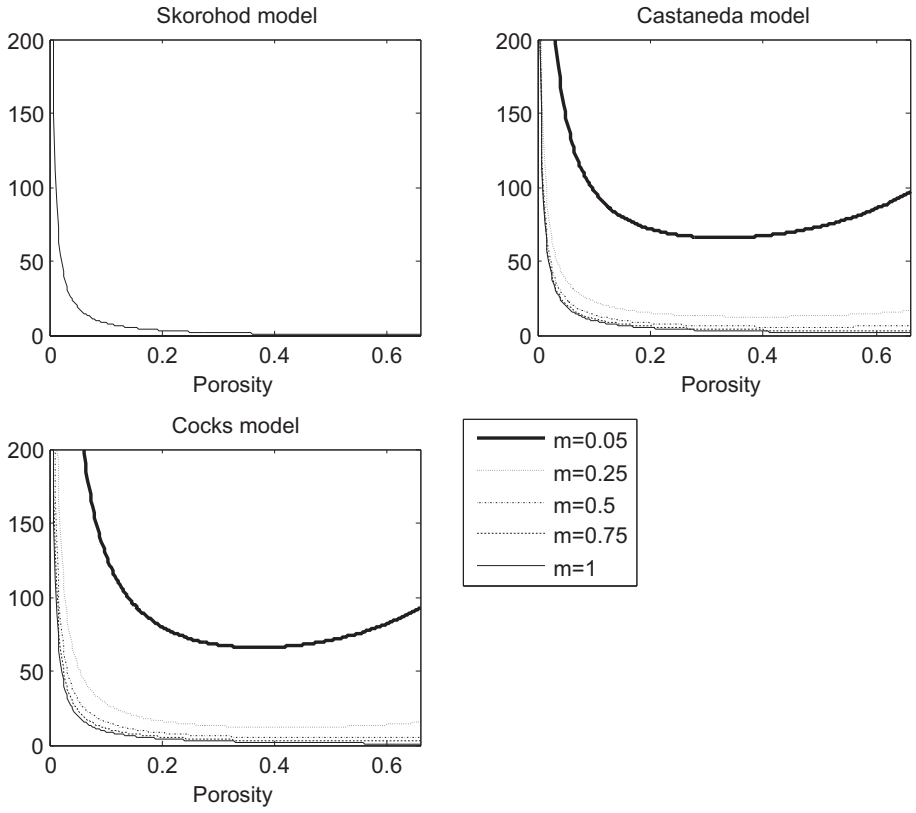

Figure 22: Normalized perturbation growth rate- Low order, S.E.P.=10

LOWorder

higherstabIP

5.2. Higher order analysis - Effect of the Laplace pressure

σ disaccoppiata dalla porosit, se perturbassi anche σ avrei un sistema di 2 equaz in 3 incognite, che ammette sempre soluzione non banale

The former analysis was meant to explore the consequences of the perturbation of the porosity on the rate of change $\dot{\theta}$, evaluated by equation (19).

Henceforth, a more refined method of producing perturbations is needed. To this end, one may follow the procedure used in [20], Section 3.1.2, owning to account for perturbation of the actual porosity and, in our case, of the Laplace pressure. It may be noticed that the quantity p_{l0} (that can be written as a function of p_L and of the porosity through equations (23) or (27)) is a material property and it does not change during the sintering process.

Two differences may be highlighted between the stability analysis performed in the present work and the one introduced in [20]:

- unlike in [20], here the high order analysis entails a process with constant external pressure;

- the presence and the perturbation of the sintering stress p_L is here considered.

A perturbed solution is considered in the following form:

$$\begin{cases} \theta(t) = \theta^{(0)}(t) + \delta\theta \exp(\lambda(t - t_0)), \\ p_l(t) = {p_l}^{(0)}(t) + \delta p_l \exp(\lambda(t - t_0)); \end{cases} \tag{33}$$

pert

by substituting (33) in equations (19) and (23) (for the Laplace pressure derived by using stochastic approach), after linearization about the foundamental solution ($\theta^{(0)}(t)$, ${p_{l0}}^{(0)}$) we have:

$$\begin{bmatrix} \frac{1}{\theta}\frac{\partial f(\theta,\sigma,p_l)}{\partial\theta} - \frac{\lambda}{\theta} & \frac{1}{\theta}\frac{\partial f(\theta,\sigma,p_l)}{\partial p_l} \\ \frac{\partial p_{l0}(\theta,p_l)}{\partial\theta} & \frac{\partial p_{l0}(\theta,p_l)}{\partial p_l} \end{bmatrix}_{\theta^{(0)}(t),{p_l}^{(0)}(t)} \begin{bmatrix} \delta\theta \\ \delta p_l \end{bmatrix} = \begin{bmatrix} 0 \\ 0 \end{bmatrix}, \tag{34}$$

systemIP

where

$$f(\theta,\sigma,p_l) = \dot{\varepsilon}_0(1-\theta)^{\frac{3m-1}{2m}}\left(\frac{|\sigma_z - p_L|}{A\sigma_0}\right)^{\frac{1}{m}}\psi^{\frac{-(1+m)}{2m}} \tag{35}$$

and the matrix appearing in (34) is evaluated at ($\theta^0(t)$, ${p_l}^0(t)$), as specified. Eq. (34) has non-trivial solutions if and only if the determinant of the matrix is equal to zero. By imposing this condition, we obtain a characteristic first-order equation with respect to the normalized perturbation growth rate $\frac{\lambda}{\dot{\theta}}$. As in the low order case, The quantity $\lambda = \frac{\delta\dot{\theta}}{\delta\theta}$ can be regarded as the perturbation growth rate. Since, during sintering, shrinkage occurs monotonically ($\dot{\theta} \leq 0$), the problem is linearly stable if the quantity $\frac{\lambda}{\dot{\theta}}$ (normalized perturbation growth rate) is negative, whereas linearly unstable if $\frac{\lambda}{\dot{\theta}} > 0$. This can be done in the framework of the three different models considered in the previous sections.

Root of equation is shown in the following figure for the three principal cases defined in section 2.1. It is evident that, since the normalized perturbation growth rate $\frac{\lambda}{\dot{\theta}}$ is negative for the whole porosity range, the sintering process is always stable. By carefully comparing figure 22 to figure 23 it can be detected that the effect of the Laplace pressure is to slightly increase the absolute value of $\frac{\lambda}{\dot{\theta}}$, i.e. to increase the stability of the process.
Figure 23 shows the results obtained considering the Laplace pressure evaluated by using the stochastic approach, leading to the following expression for the sintering stress: $p_L = \frac{3\alpha}{r0}(1-\theta)^2$. Results obtained by using the other methodology (that leads to $p_L = \frac{2\alpha}{r0}\sqrt{\frac{2}{3}\psi(\theta)\frac{\theta}{1-\theta}}$) are very similar.

higherstabIP_PI

5.3. Higher order analysis - Effect of the gas pressure in the pores

In the present subsection, a coupled perturbation of the porosity evolution rate, Laplace pressure and gas pressure in the pores p_i is introduced, in order to investigate the effect of p_i on the stability of the sintering process. A perturbed solution is considered in the following form:

$$\begin{cases} \theta(t) = \theta^{(0)}(t) + \delta\theta \exp(\lambda(t - t_0)), \\ p_l(t) = {p_l}^{(0)}(t) + \delta p_{l0} \exp(\lambda(t - t_0)), \\ p_i(t) = {p_i}^{(0)}(t) + \delta p_i \exp(\lambda(t - t_0)). \end{cases} \tag{36}$$

pertPI

Such a perturbed solution is substituted in the governing equations of the problem: (19), (23) (for the Laplace pressure derived by using stochastic approach) or (27)

(for Laplace pressure obtained through dissipative approach) and (29). Note that the external pressure at the pore closure, p_0, is a fixed parameter. After a linearization about the foundamental solution $(\theta^{(0)}(t),\ {p_i}^{(0)},\ {p_{l0}}^{(0)})$, the following set of equations can be obtained:

$$\left[\begin{array}{ccc} \frac{1}{\theta}\frac{\partial f(\theta,\sigma,p_l)}{\partial\theta} - \frac{\lambda}{\theta} & \frac{1}{\theta}\frac{\partial f(\theta,\sigma,p_l)}{\partial p_l} & \frac{1}{\theta}\frac{\partial f(\theta,\sigma,p_l)}{\partial p_i} \\ \frac{\partial p_{l0}(\theta,p_l)}{\partial\theta} & \frac{\partial p_{l0}(\theta,p_l)}{\partial p_l} & 0 \\ \frac{\partial p_0(\theta,p_i)}{\partial\theta} & 0 & \frac{\partial p_0(\theta,p_i)}{\partial p_i} \end{array}\right]_{\theta^{(0)}(t),{p_l}^{(0)}(t),{p_i}^{(0)}(t)} \left[\begin{array}{c} \delta\theta \\ \delta p_l \end{array}\right] = \left[\begin{array}{c} 0 \\ 0 \\ 0 \end{array}\right]. \tag{37}$$

systemIP_PI

As in the previous subsection, in order to obtain non trivial solutions of (37), the determinant of the matrix has to be null. By imposing such a condition, a first-order equation with respect to the normalized perturbation growth rate $\frac{\lambda}{\theta}$. As in the previous cases, the problem is linearly stable if the quantity $\frac{\lambda}{\theta}$ (normalized perturbation growth rate) is negative, whereas linearly unstable if $\frac{\lambda}{\theta} > 0$. The normalized perturbation growth rate is plotted in figure 24 as a function of the porosity, for different values of m and for Skorohod, Castaneda-Mc Meeking and Cocks models. Obviously, the presence of p_i influences just the third phase of the sintering process, for relative densities greater than 90%, i.e. for $\theta < \theta_C = 0.1$. Moreover, the final porosity θ^* is

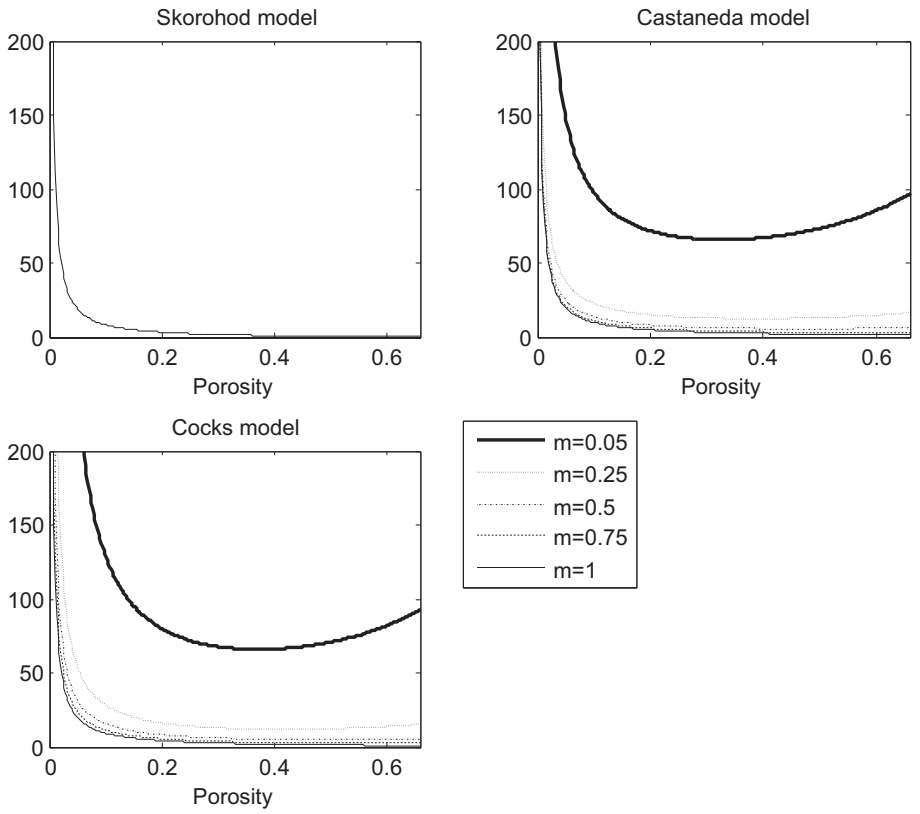

Figure 23: Normalized perturbation growth rate - High order stability analysis, S.E.P.=10

HIGHorderPL

here greater than zero, and it depends upon the applied external pressure.

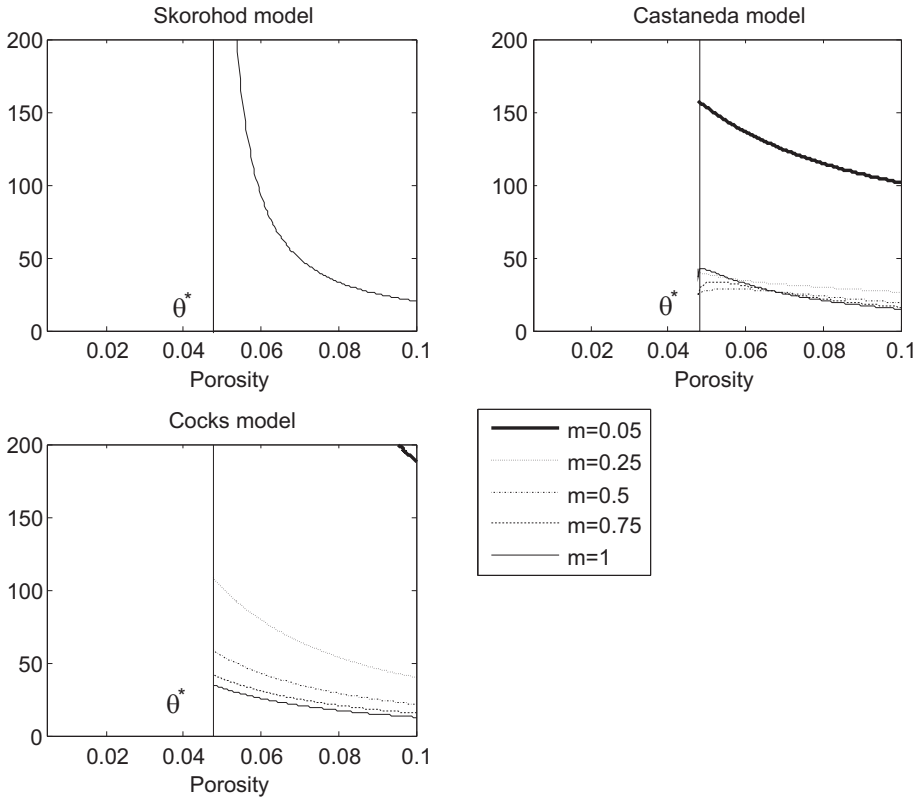

Figure 24: Normalized perturbation growth rate - High order stability analysis, S.E.P.=2 HIGHorderPLPI

As it is evident from figure 24, the effect of the gas pressure in the pores is to reduce the value of the normalized perturbation growth rate $\frac{\lambda}{\dot{\theta}}$, i.e. to reduce the stability of the sintering process. Nevertheless, the process turns out to be stable.

Figure 24 shows the results obtained considering the Laplace pressure evaluated by using the stochastic approach, leading to the following expression for the sintering stress: $p_L = \frac{3\alpha}{r0}(1-\theta)^2$. Results obtained by using the other methodology (that leads to $p_L = \frac{2\alpha}{r0}\sqrt{\frac{2}{3}\psi(\theta)\frac{\theta}{1-\theta}}$) are qualitatively very similar.

ashby74 [1] Ashby, M. F., 1974. A first report on sintering diagrams. Acta Metallurgica 22, 275-289.

ashby [2] Ashby, M.F., Background Reading, HIP 6.0. *University of Cambridge, Cambridge, UK.* (1990)

artz [3] Artz, E., Ashby, M. F., Easterling, K. E.,Pratical applications of hot-isostatic pressing diagrams: four case studies, *Metallugical Transaction A*, **14A** (1983) 211-221.

cocks93 [4] Cocks, A.C.F., The structure of constitutive laws for the sintering of fine grained materials, *Acta Metallurgica et Materialia* **42** (1994) 2191-2210.

cocks [5] Cocks, A.C.F., The structure of constitutive laws for the sintering of fine grained materials. *Overview No. 117. Acta Metall.* **42(7)** (1994) 2191.

coleman [6] Coleman, S. C., Beere, W., The sintering of open and closed porosity in UO_2, *Journal of applied physics*, **41** (1970) 4798-4807.

Duva [7] Duva, J.M., Crow, P.D.. The densification of powders by power-law creep during hot isostatic pressing. *Acta Metall.***40(1)**(1992) 31-35.

mat3 [8] A. Gke, F. Findik, Mechanical and physical properties of sintered aluminum powders,Journal of Achievements in Materials and Manufacturing Engineering, Volume 30 Issue 2 October (2008)

Green [9] Green, D.J., Guillon, O., Rdel, J, 2008. Constrained sintering: A delicate balance of scales. Journal of the European Ceramic Society, 28(7), 1451-1466.

Guillon [10] Guillon, O., Cao, S., Chang, J., Wondraczek, L., Boccaccini, A.R., 2011. Effect of uniaxial load on the sintering behaviour of 45S5 Bioglass powder compacts. Journal of the European Ceramic Society 31, 999-1007.

hutchinson [11] J.W.Hutchinson, K. Neale, A. Needleman, Sheet necking I- validity of plane stress assumptions on the long-wavelenght approximation, in: Koistinen, D.P., Wong, N.M. (Eds.), Mechanics of Sheet Metal Forming, vol.1. Plenum, NY, pp.111-126. (1978)

alpha [12] V.K.Kumikov, Kh.B. Khokonov, On the measurement of surface free energy and surface tension of solid metals. *Journal of Applied Phisics.* **54(3)**,(1983),1346-1350.

lee [13] Lee, J.-S., Klinger, L., Rabkin, E., 2012. Particle rearrangement during sintering of heterogeneous powder mixtures: A combined experimental and theoretical study. Acta Materialia 60(1), 123-130.

olevskymax [14] Maximenko, A., Olevsky, E., 2005. Homogeneity of isostatic pressure-assisted sintering of agglomerated powder, International Journal of Solids and Structures 42(2), 503-515.

maximenko [15] Maximenko, A., Kuzmov, A., Grigoryev, E., Olevsky, E., 2012. Direct Multi-Scale Modeling of Sintering. Journal of the American Ceramic Society 95(8), 23832388.

mat1 [16] Muhlberg M., Paschen P.,Liquid phase sintering of AlZnMgCu alloys, Zeitschrift fr Metallkunde ISSN 0044-3093 (1993), vol. 84, no5, pp. 346-350

Munir [17] Munir, Z.A., Anselmi-Tamburini, U., Ohyanagi, M., 2006. The effect of electric field and pressure on the synthesis and consolidation of materials: A review of the spark plasma sintering method. Journal of Materials Science 41(3), 763-777.

rewiev [18] Olevsky, E.A., Theory of sintering: from discrete to continuum. *Invited Review. Mater. Sci. Eng. Rep. Rev.* **23** (1998) 41-100.

olevsky2 [19] Olevsky, E.A., Molinari, A., Instability of sintering of porous bodies. *Int. J. Plast* **16** (2000) 1-37.

olevsky1 [20] Olevsky, E.A., Molinari, A., Kinetics and stability in compressive and tensile loading of porous bodies. *Mechanics of Materials* **38** (2006) 340-366.

Olevsky2006 [21] Olevsky, E.A., Tikare, V., Garino, T., 2006. Multi-Scale Study of Sintering: A Review. Journal of The American Ceramic Society 89(6), 1914-1922.

castaneda [22] Ponte Castaneda, P., The effective mechanical properties of nonlinear isotropic composites. *J. Mech. Phys. Solids* **39** (1991) 45.

Sankar [23] Sankar, U., Satgunam, M., Amiriyan, M., Singh, R., Teng, W.D., 2011. Sintering and Densification Behavior of ZnO-Doped Y-TZP Ceramics. Applied Mechanics and Materials 83, 197-203.

mat2 [24] G.Schaffer et al., The effect of trace elements on the sintering of an Al-Zn-Mg-Cu ALLOY Acta Materialia, Volume 49, Issue 14, Pages 2671-2678 (2001)

Scherer [25] Scherer, G.W. , 2001. Viscous Sintering. Encyclopedia of Materials: Science and Technology, 95369540.

skorohod [26] Skorohod, V.V., Rheological Basis of the Theory of Sintering. *Naukova Dumka, Kiev.* (1972) .

mcmeeking [27] Sofronis, P., McMeeking, R.M., Creep of power-law material containing spherical voids. *Trans. ASME* **59** (1992) 88-95.

Schwarz [28] Schwarz, S., Thron, A.M., Rufner, J., van Benthem, K., Guillon, O., 2012. Low Temperature Sintering of Nanocrystalline Zinc Oxide: Effect of Heating Rate Achieved by Field Assisted Sintering/Spark Plasma Sintering. Journal of the American Ceramic Society 95(8), 24512457.

ashby80 [29] Swinkels, F.B., Ashby, M. F., A second report on sintering diagrams, *Acta Metallurgica*, **29** (1980) 259-281.

ashby83 [30] Swinkels, F.B., Wilkinson, D.S., Artz, E., Ashby, M. F., Mechanisms of hot isostatic pressing, *Acta Metallurgica*, **31(11)** (1983) 1829-1840.

Wakai2007 [31] Wakai, F., Chihara, K., Yoshida, M., 2007. Anisotropic shrinkage induced by particle rearrangement in sintering. Acta Materialia 55(13), 4553-4566.

Wakai [32] Wakai, F., 2013. Mechanics of viscous sintering on the micro- and macro-scale. Acta Materialia 61(1), 239-247.

wilkinson [33] Wilkinson, D. S., A pressure-sintering model for the densification of polar firn and glacer ice, Journal of glaciology, **34(116)** (1988) 40-45.

Wolff [34] Wolff, C., Mercier, S., Couque, H., Molinari, A., 2012. Modeling of conventional hot compaction and Spark Plasma Sintering based on modified micromechanical models of porous materials. Mechanics of Materials 49, 72-91.

6. Conclusion

Appendix A. Free sintering

freeS

The case of free sintering corresponds to a condition frequently met in industrial processes. In these cases, there is no applied external pressure, so that the shrinkage is due to the sintering stress p_L only.

In the case under examination, the stress and strain-rate tensors are purely hydrostatic. Thus, free sintering can be seen as a particular case of isostatic pressing, with null external loading stress. The evolution law for the porosity may be obtained from eq.(19), by substituting $\sigma = 0$:

$$\dot{\theta} = -\Big(\frac{p_L - p_i}{\sigma_0 A}\Big)^{\frac{1}{m}} \dot{\varepsilon_0} \psi^{\frac{-(1+m)}{2m}} (1-\theta)^{\frac{3m-1}{2m}}. \tag{A.1}$$

thetafree

The introduction of the dimensionless specific time τ_L, defined by equation (20), yields the following normalization of equation (A.1):

$$\frac{\partial \theta}{\partial \tau_L} = (p_L - p_i)^{\frac{1}{m}} \psi^{\frac{-(1+m)}{2m}} (1-\theta)^{\frac{3m-1}{2m}}. \tag{A.2}$$

thetafreeADIM

Appendix A.1. Effect of the Laplace pressure

Because for free sintering, since the gas pressure in the pores is neglected, the only force driving the process is the Laplace pressure, it is worth noting that the choice of the approach used to derive its expression (stochastic or dissipation averaging, see section 2.2) has a strong influence on the result. This issue may be studied in the sequel.

1. *Sintering stress by using a stochastic approach ($p_L = \frac{3\alpha}{r_0}(1-\theta)^2$, see section 2.3.1)*
   By substituting the expression $p_L = \frac{3\alpha}{r_0}(1-\theta)^2$, equation (A.2) can be written as follows:
   $$\frac{\partial \theta}{\partial \tau_L} = \Big(\frac{3\alpha}{r_0}\Big)^{\frac{1}{m}} \psi^{\frac{-(1+m)}{2m}} (1-\theta)^{3(\frac{m+1}{2m})}. \tag{A.3}$$
   thetafreeADIM2
   In order to compare the evolution of the porosity, for such a case, for the three different models considered in section 2.2 (Skorohod, Cocks, Castaneda-Duva-Crow and Mc Meeeking; the latter two models coincide for isostatic pressing), Figure A.1 shows the evolution of the porosity for different values of the strain rate sensitivity m.

   It is worth noting that the result obtained for the three considered model are fairly different. This is due to the different expressions of the bulk modulus ψ.
   Figure 2 (section 2.2) shows that the model of Cocks, for m=1, gives the highest values of ψ in all range of interesting porosities. For such values of ψ, equation (A.3) gives lower values of the rate of change of the porosity $\dot{\theta}$ and it corresponds to higher sintering times.
   Because the model of Skorohod introduces the smaller values of ψ, the sintering times obtained by adopting such a model are the shortest.
   In Figure A.1 the different $\dot{\theta}$ are plotted for the models of Castaneda and Mc Meeking,

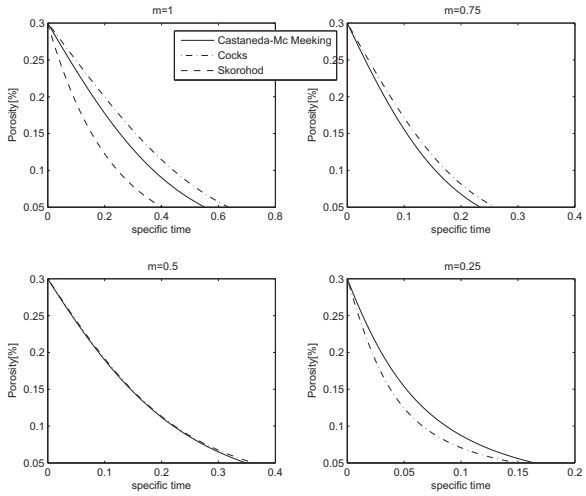

Figure A.1: Free Sintering-Evolution of Porosity for different values of m , $p_L = \frac{3\alpha}{r_0}(1-\theta)^2$

FS2

.

for different values of the parameter m.
Whenever m decreases, Figure 2 (section 2.2) shows that values of the bulk modulus ψ obtained by using the model of Castaneda increase, whereas the ones coming from the model of Cocks decrease. The same figure shows that, for lower values of m, the model of Castaneda gives values of ψ lower than the ones obtained by using the Cocks expression for the same item. Hence, the employment of the model of Cocks gives sintering times lower than those ones obtained by using the approach of Castaneda. From Figure A.1, it may also be worth noting that, when m tends to zero (ideal plastic behavior), the time-porosity graph has a steep knee.

2. *Sintering stress from dissipation averaging (i.e.* $p_L = \frac{2\alpha}{r_0}\sqrt{\frac{3}{2}\psi(\theta)\frac{\theta}{1-\theta}}$*, see section 2.3.2)*
In this case, expression (A.1), which holds for m=1 only, reduces to

$$\dot{\theta} = -\frac{\dot{\varepsilon_0}}{\sigma_0 A}\frac{2\alpha}{r_0}\sqrt{\frac{3}{2}\frac{\theta(1-\theta)}{\psi}}. \qquad \text{(A.4)}$$

efree1

In the considered range of porosity, the resulting values of the Laplace pressure may be shown to be lower than the ones obtained by virtue of the expression derived by the stochastic approach (see Figure 5) and henceforth the sintering times are higher.

Appendix A.2. Effect of the gas pressure in the pores

In the case of free sintering, the stress due to the external (relative) pressure is $\sigma = 0$; the total driving force of the problem is thus given by the sum of a positive contribute, the Laplace pressure p_L, and the gas pressure in the pores, that gives a "negative" contribute. Since the applied external pressure is equal to the standard atmospheric pressure, at the closure porosity θ_C, $p_i = 0$. Hence, the gas pressure in the pores is usually negligible with respect to the interstitial pressure p_L and the condition (31) is not reached. More precisely, it can be

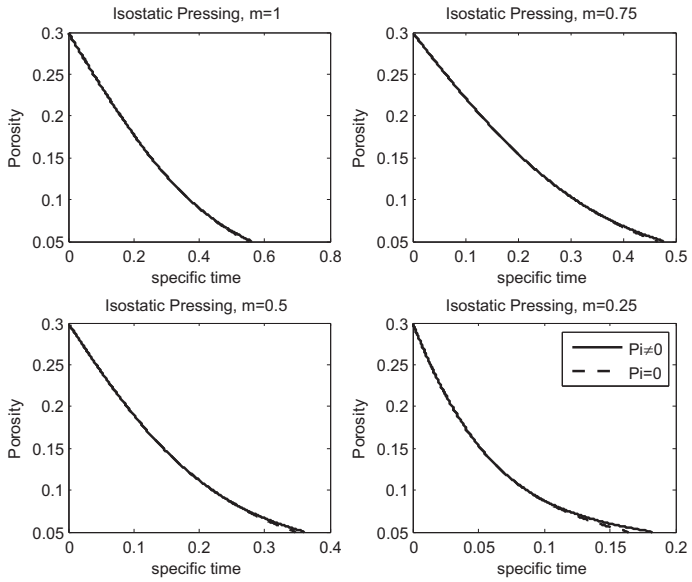

Figure A.2: Free Sintering-Evolution of Porosity for different values of m

freePI

.

attained for values of grain size not used in real sintering processes.

Figure A.2 shows the evolution of the porosity for a free sintering process in two cases:

- accounting for the whole driving force (dashed line) $-p_L + p_i$;
- neglecting the gas pressure in the pores (dotted line), i.e. the driving force is considered to be only p_L .

It is evident that the gap between the two curves is negligible.

Appendix A.3. Influence of the temperature on the free sintering time

In this paper, the sintering processes are assumed to be at constant temperature. In fact, pre-heated electric oven are employed in industrial processes, whose thermal capacity may be regarded infinitely large with respect to the one of any specimen under consideration. Henceforth, the temperature remains constant during sintering.
In this section, temperatures are normalized by using the dimensionless specific temperature $T*$, defined as:

$$T^* := \frac{T}{T_{melting}}. \tag{A.5}$$

There are two main phenomena that determine the influence of the temperature on free sintering processes:

1. for lower values of m ($m \to 0$), the material behavior is almost plastic and yet it feels the effects of the temperature more than for higher values of the parameter m (see Figure A.3).
2. the material behavior is affected by the temperature; thus the values of the parameter m should be a function of the temperature.

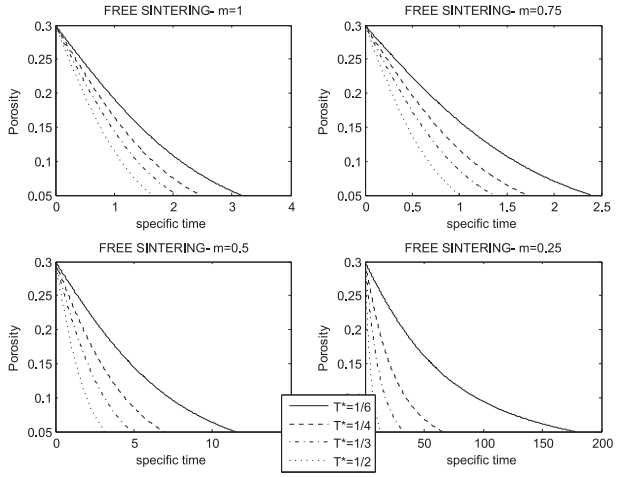

Figure A.3: Free sintering-Evolution of porosity for different values of the specific temperature.

temperatura

The present model takes only into account the first phenomenon, and the implicit dependence on the temperature is given by $A = \tilde{A}(T)$ (see [2]) and the material constant A, appearing in equation (A.1), is raised to $1/m$.
Figure A.3 shows the evolution of the porosity, evaluated by using the model of Castaneda and for the expression of p_L derived by the stochastic approach, for different values of the strain rate sensitivity m and for different specific temperature T^*. It is evident that, when the temperature increases, the sintering time does decrease. This reduction becomes more important for lower values of the parameter m.